zürich 2024

FDD

European Hyperloop Week

Tachyon Hyperloop

March 17, 2024

EUROPEAN HYPERLOOP WEEK

Contents

Traction System

1.1 Introduction

The traction system of the Hyperloop pod plays a pivotal role in ensuring the efficient transmission of power to the ground, facilitating the acceleration, and maintaining high-speed stability. This system is intricately designed to optimize the pod's grip and minimize slippage, particularly during high-speed operations and in varying track conditions.

Key considerations for the traction system include the selection of materials and technologies that maximize frictional force while minimizing wear and energy loss. Additionally, the system must be robust enough to handle the dynamic loads and stresses encountered during rapid acceleration, sustained high-speed travel, and deceleration phases.

In this section, we will delve into the specifics of the traction system, exploring its components, design considerations, and the integration with the overall pod architecture. The focus will be on ensuring that the system contributes to the overall efficiency, safety, and performance of the Hyperloop pod, aligning with the project's goals of high-speed and sustainable transportation.

1.2 Propulsion

1.2.1 Overview

To accelerate our Hyperloopod we use our EMRAX 188 electric motor from last season. This delivers an output of 60 kW under high voltage and a maximum torque of 100 Nm. This torque gets transferred to a right-angle gearbox and from there is slid to the drive wheels via cardan joints.

Concept

The main goal of this system is to accelerate our pod with an acceleration of $5\,\mathrm{m/s^2}$. Since the given $100\,\mathrm{Nm}$ are not sufficient under an estimated total weight of $250\,\mathrm{kg}$, the drivetrain requires a gear ratio. Since an angular gearbox is installed anyway, it is easy to implement this criterion there. In order to maintain a relatively high top speed of the pod, this transmission ratio should be as close as possible. According to the formula

$$T_{\text{required}} = \frac{(m \cdot a + \frac{1}{2} \cdot \rho_{\text{air}} \cdot C_w \cdot A_{\text{Aeroshell}} \cdot v^2 + m \cdot g \cdot \cos(\Theta)) \cdot r}{\eta}$$

we know that we require at least around $170\,\mathrm{Nm}$ of torque to achieve this amount of acceleration. While the pod weight of $250\,\mathrm{kg}$ is only an estimate at the time of system design and we are always keen to get such complex parts from our partners, we opted for a $2:1$ ratio of a Mädler gearbox. With this gear ratio, a respectable top speed of $113\,\mathrm{km/h}$ is still possible. This is absolutely sufficient

for our prototype, as we are still sticking to our basic idea: For low speeds and accelerations, we drive our hyperloop pod with a conventional wheel drive and for everything above that, the pod will hover with a linear induction motor which will be added in future prototypes. We believe that we can achieve an increase in efficiency in this way as permanent levitation is not necessary.

The transmitted torque must now be directed to the drive wheels in such a way that it is still possible to ensure a working suspension. For this, we use universal joints on both sides of the centered bevel gear. These also come from our partner Mädler and are connected to the bevel gear using in-house produced adapter shafts and feather keys. To finally connect the other ends of the shaft joints to the wheel, only one last shaft is missing. This is also fitted with a keyway on the joint side and a bolt circle on a flange on the wheel side. Now that the wheels are supplied with power, it is important to create sufficient rolling friction. To achieve this, Continental provides us with a rubber coating for our wheels.
Of course, this all has to be mounted into the chassis. For this, we use three different types of brackets beside the knuckles, where the wheelshafts are mounted: one for the motor, one for the motorshaft and two of the same kind, which carry everything between the shaft joints.

Size, Components, and Appearance

Table 1.4

Component	Number	Mass [kg]	Size [mm]	In-house/ outsourced
Motor	x1	7	$188 \times 188 \times 112$	Bought
Motorshaft	x1	0.4	$170 \times 83 \times 83$	Outsourced
Bevelgear z=20	x1	3	10×90	Bought
Bevelgear z=40	x1	9.6	$20 \times 30 \times 50$	Bought
Gearshaft Pressfitted	x1	0.3	$103 \times 40 \times 40$	Outsourced
Gearshaft bolted	x1	0.7	$106 \times 55 \times 55$	Outsourced
Shaft Joint	x2	4.1	$30 \times 40 \times 60$	Bought
Wheelshaft	x2	0.7	$138 \times 100 \times 100$	Outsourced
Wheel	x2	1.7	$200 \times 200 \times 155$	Outsourced

Table 1.1: Components

1.2.2 Design Process and Appearance

Motor

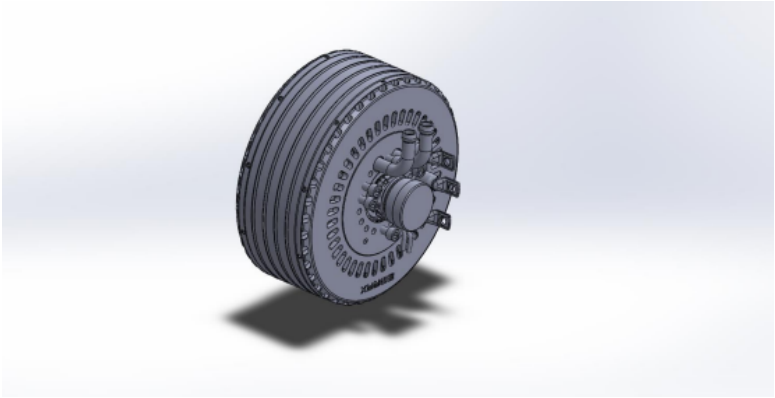

Figure 1.1: CAD of EMRAX 188

As previously mentioned, we are once again using our EMARX 188 electric motor from last season. You can find all the technical details in Table 1.23 .

Motorshaft

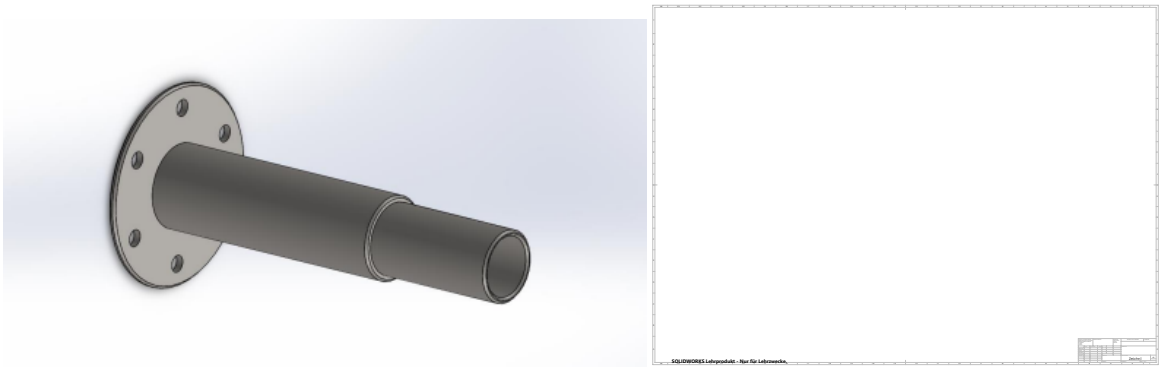

(a) CAD Render (b) Technical Drawing

Figure 1.2: Motor Bracket

Even though it is a heavy material, C45 steel provides adequate tensile strength to transmit torque from the motor to the gearbox or from the gearbox to the wheels. To maintain a relatively low weight for this part, it is hollow like all the other shafts. In Figure 1.3, you can now see the applied forces. The shaft is mounted on the motor at the screw holes of the flange (green). This means that the motor torque of 100 Nm (pink) acts up to the surface on which the bevel gear is pressed. The calculation of the contact pressure of 16.26 MPa is given by

$$p_{\text{contact}} = \frac{2 \cdot M \cdot S_r}{\pi \cdot D^2 \cdot l \cdot \mu}$$

In addition, there is a centrifugal force (blue) at maximum rotational speed of 6000 rpm.

Figure 1.3

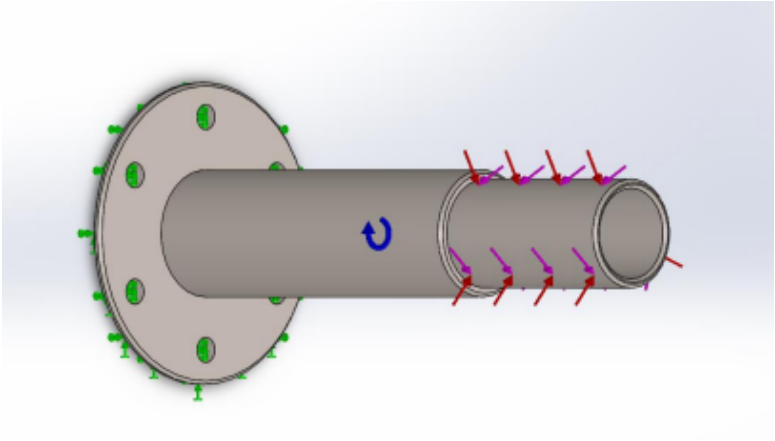

Figure 1.3: Forces acting on the Motorshaft

Bevel Gears

picture gearbox

The bevel gears with the article numbers 36736000 and 36736100 are our choice to fulfill the desired purpose. 36736000 offers spur gearing with 20 teeth. With a maximum permissible torque of 130 Nm, it can withstand the prevailing forces. The larger counterpart 36736100 therefore has twice as many teeth (40 teeth) and is designed for a maximum torque of 260 Nm.

Gearshafts

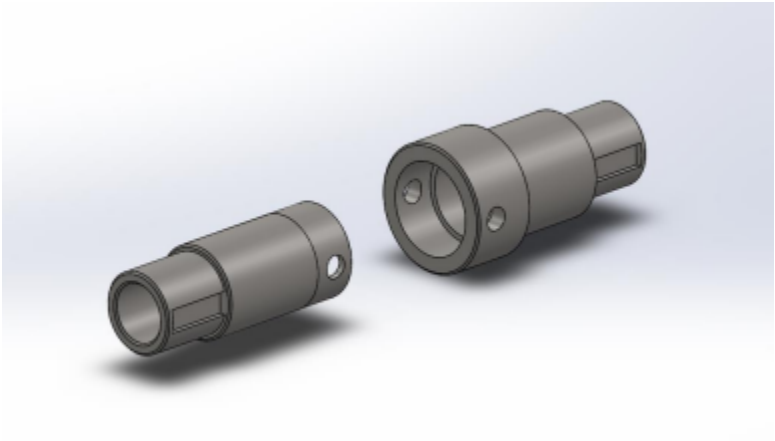

Figure 1.4

To be able to conduct the torque of the bevel gear, we have designed another shaft. This consists of two individual parts, one which is again pressed into the bevel gear and the other which is screwed onto the first part after pressing. The specifications of the initially acting shaft are as follows:

Fig.xx shows all the acting forces. For calculating the pressing force (red) we again use the formula for p_{contact} and get the result of 21.22 MPa. The higher torque of 200 Nm (pink) resulting from the gear ratio also acts on this surface and is transferred to the screw holes and keyway (green). A centrifugal force (blue) also acts on this part, but this has now been halved by the gear ratio and is therefore only based on 3000 rpm. Finally, we assume a bearing restraint (orange) at the shaft end to the shaft joint. The admissibility of this case is described in the paragraph on the shaft joint itself.

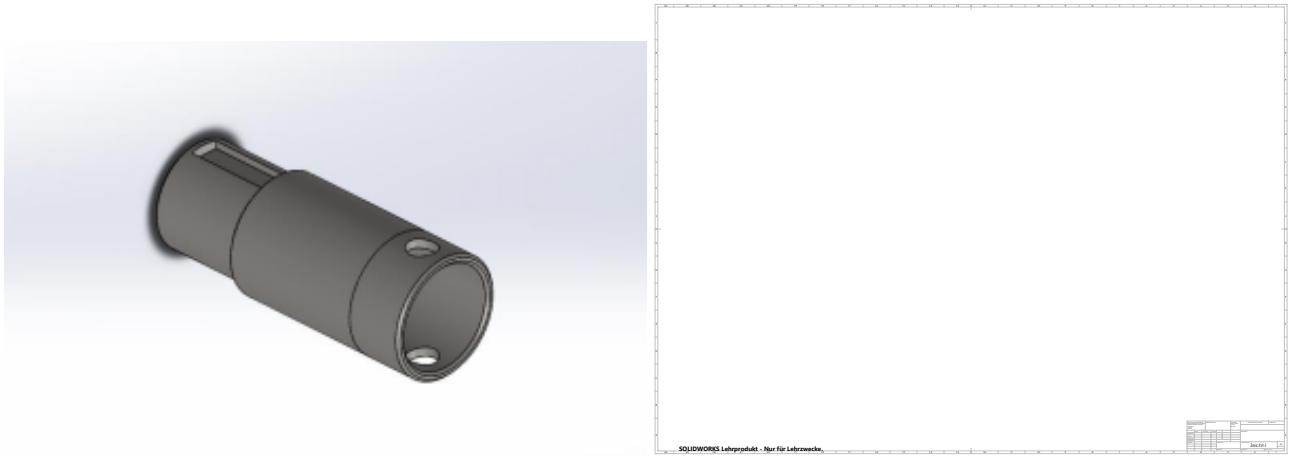

(a) CAD Render (b) Technical Drawing

Figure 1.5: Motor Bracket

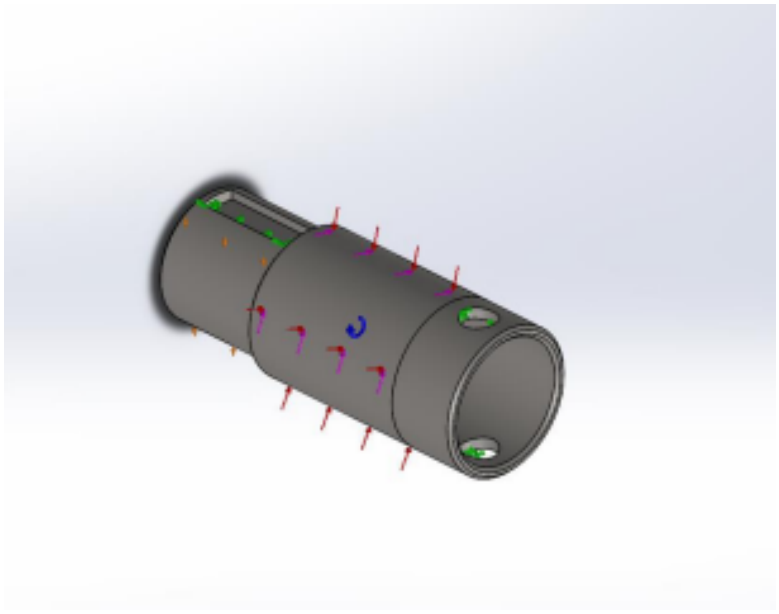

Figure 1.6: Forces acting on the pressfitted Gearshaft

The torque is now transferred to the second part of the gearshaft:

Fig.xx shows all the forces acting on this part. The two shafts are connected to each other at the screw holes (green). The centrifugal force (blue) acts as in the first shaft at 3000 rpm and the torque of 200 Nm (pink) up to the keyway. This end piece of the shaft is also simulated as a bearing (orange).

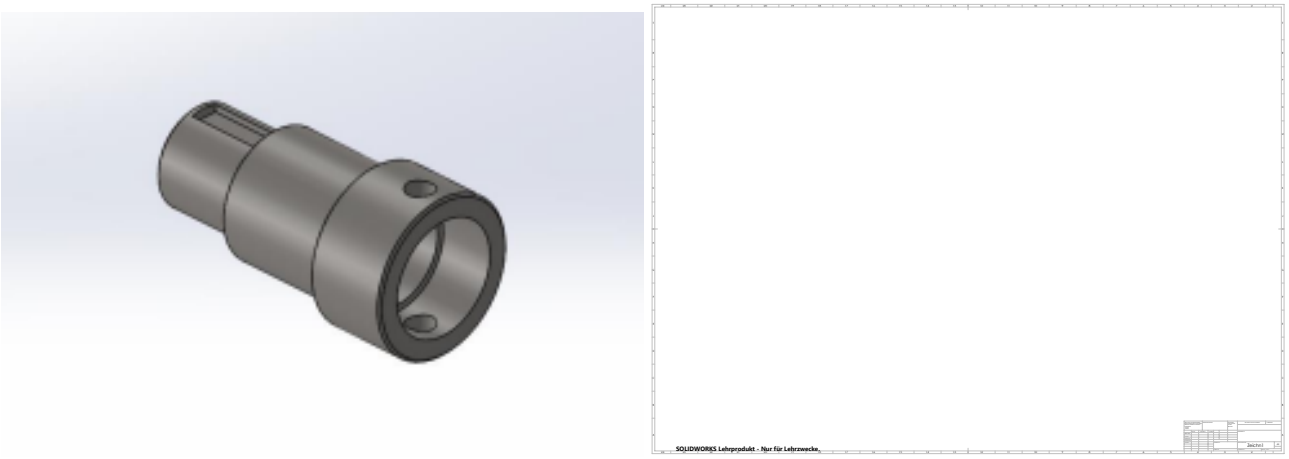

(a) CAD Render (b) Technical Drawing

Figure 1.7: Motor Bracket

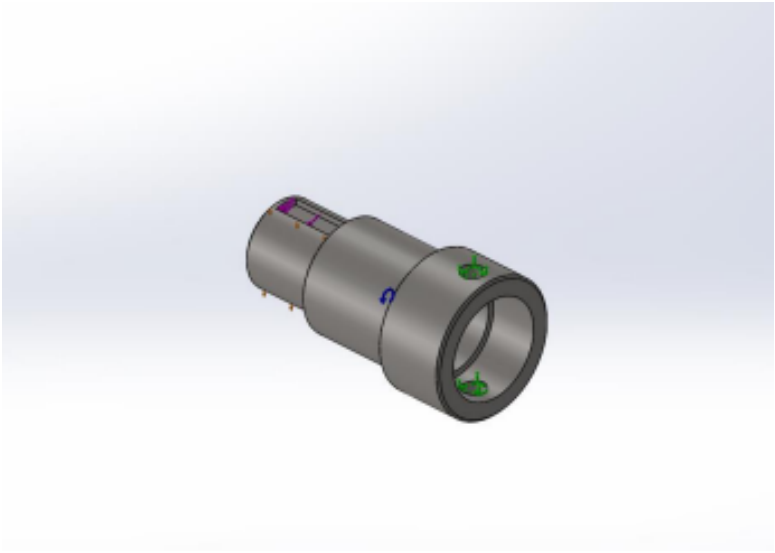

Figure 1.8: Forces acting on the bolted Gearshaft

Shaft Joints

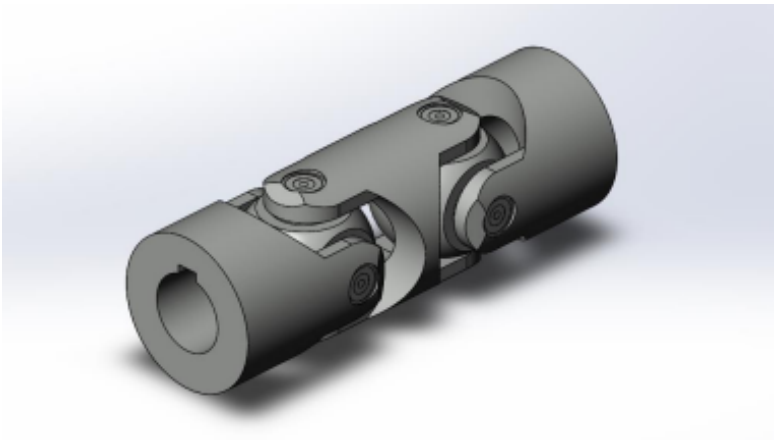

Figure 1.9

To enable the system to absorb shocks, we use cardan shafts on each side. This allows the wheels to move vertically independently of the rest of the pod. Our partner Mädler is once again supplying us with such complex parts. Item number 6 3167000N is a double universal joint which we install in our system. It has a keyway at both ends and is designed to transmit 202 Nm at 3000 rpm. These specifications are almost perfect for our drive power. We will mount the heart of our system at the ends of this joint adjacent to the gearbox. This is also the reason why a bearing is created at the respective ends in the simulations of the shafts because this bearing is also attached above the respective area. However, more on the bearing and attachment points will follow in the corresponding sections.

Wheelshafts

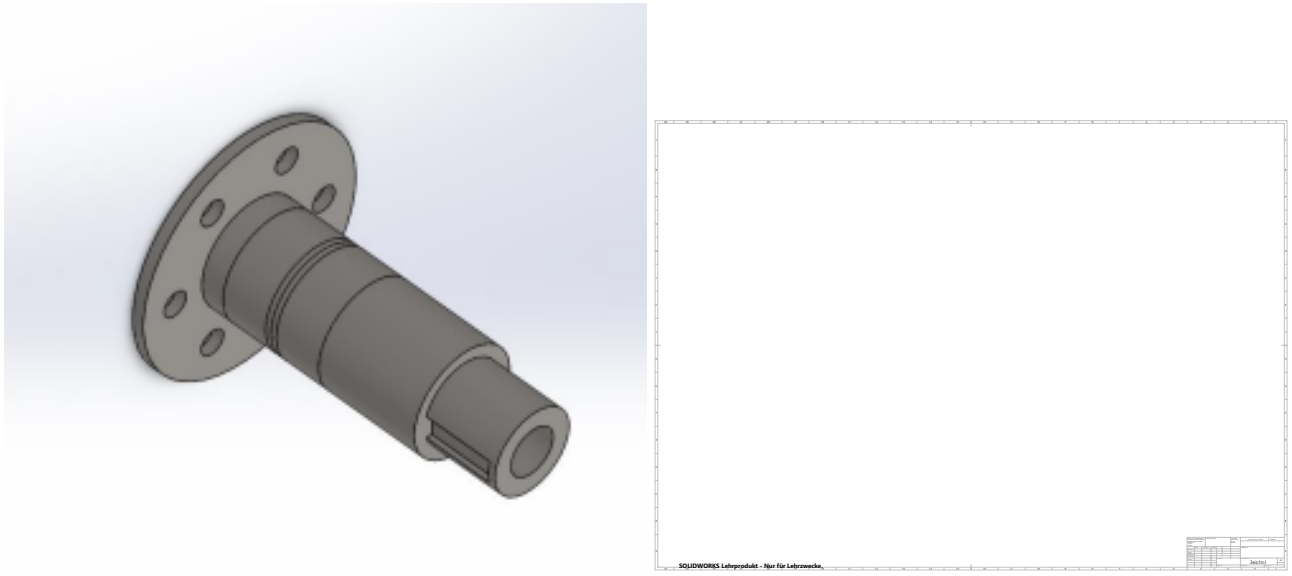

(a) CAD Render (b) Technical Drawing

Figure 1.10: Motor Bracket

The wheel shafts provide the mounting point for the wheels. This is done by means of a bolt circle on a flange to ensure easy mounting and, if necessary, changing of the wheels. In this shaft, the 200 Nm torque (pink) applied to the keyway is transmitted to the wheel over the entire surface of the flange. The centrifugal force (blue) is also generated again due to the 3000 rpm and this shaft is also mounted on bearings (orange) within the knuckles. You can find out more about this bearing in the suspension section. However, this shaft must be able to withstand the mass inertia of the wheel (red). This is calculated by $5/2 \times m_{\text{wheel}} \times a$

Wheels

Finally, we transfer the torque (pink) to the wheels via the contact surface of the flange (green). The mass inertia of the wheel (red) $5/2 \times m_{\text{wheel}} \times a$, again the centrifugal force at 3000 rpm (blue) and the local pod weight of approximately 600 N (orange) also have an effect here. This weight, together with the rolling friction coefficient of the rubber cover, enables slip-free propulsion. We get this coefficient of 0,5099 by the formula

$$\frac{m \cdot a}{m \cdot g}$$

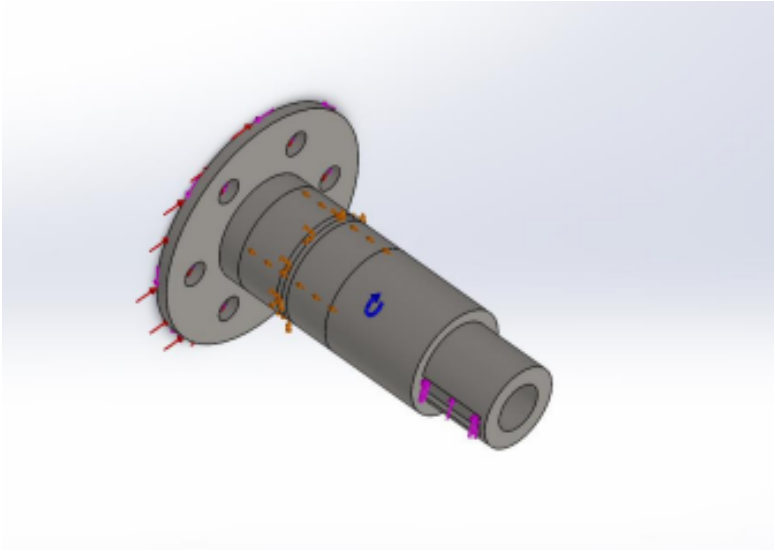

Figure 1.11: Forces acting on the wheelshaft

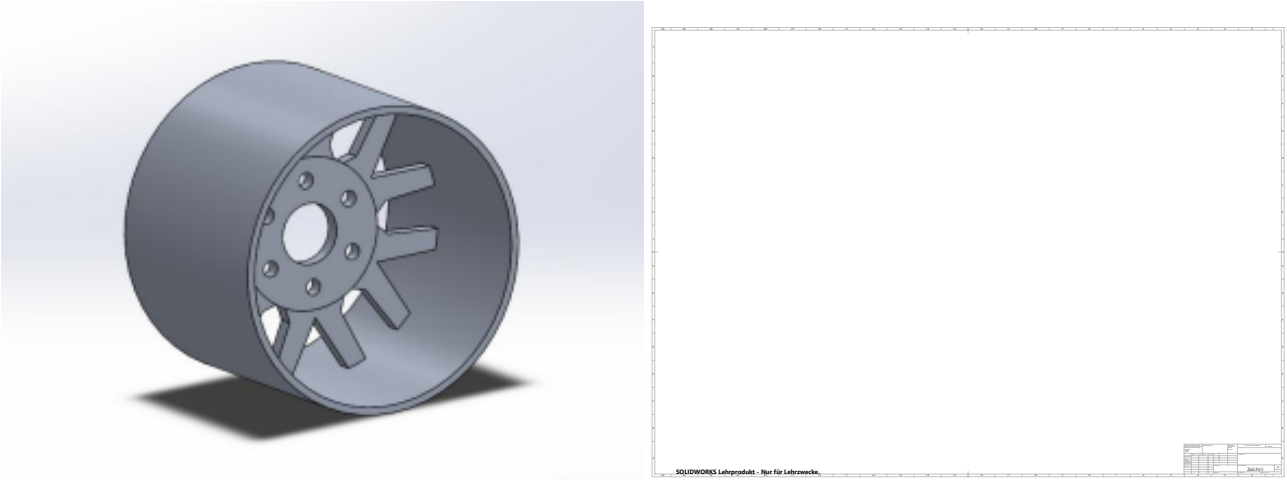

(a) CAD Render (b) Technical Drawing

Figure 1.12: Motor Bracket

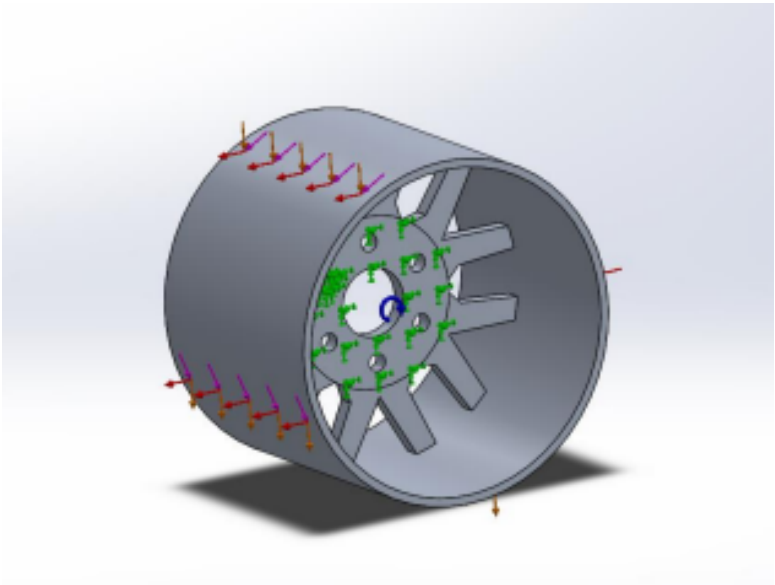

Figure 1.13: Forces acting on the wheels

Motorbracket

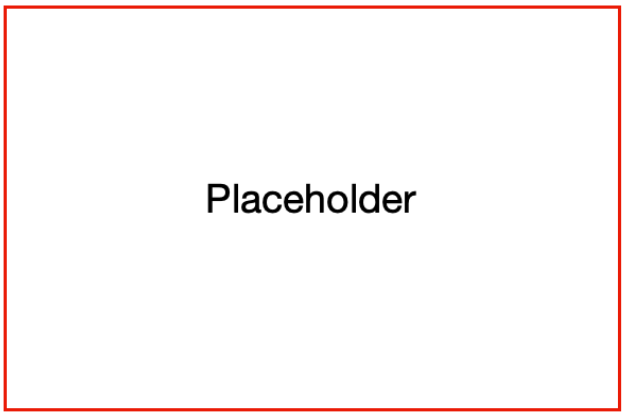

(a) CAD Render

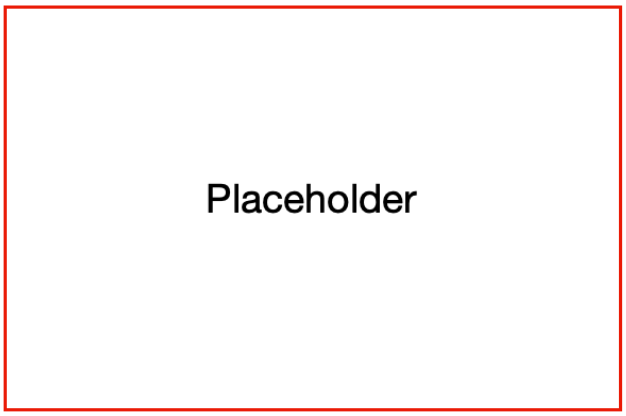

(b) Technical Drawing

Figure 1.14: Motor Bracket

Our motor is mounted in the chassis using a bracket. This contains all the holes for screws and other components that protrude to the rear. End plates with screw holes are welded to four arms to finally screw () them into the chassis. The torque () and the inertia of the motor () prevail at this bracket.

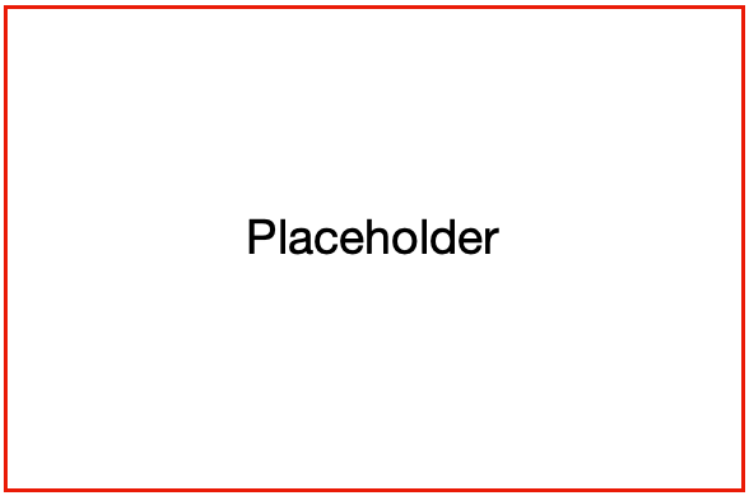

Figure 1.15: Forces acting on the motorbracket

Motorshaftbracket

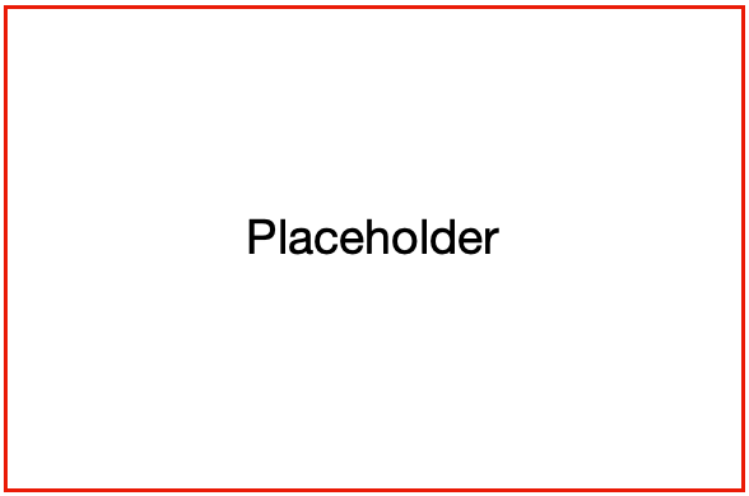

Figure 1.16

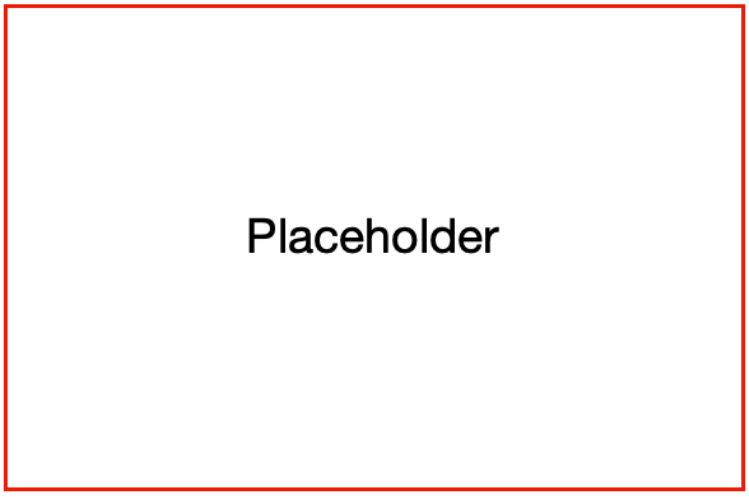

Figure 1.17

To finally support this first area of the drive system, we also support the shaft that protrudes from the motor. This is done using the CHDF35 flangebearing from Misumi. This bearing is finally integrated into the chassis by another bracket. Only the weight of the motor shaft (), its mass inertia and the wheight of the flangebearing () act on this bracket.

Bearinghouse

To provide sufficient support for the drive axle, we mount it at two points. For space reasons, we designed the bearinghouse ourselves. The weight of the axle (pink) acts on this bearinghouse at the respective point, as well as its mass moment of inertia (). This bearing shell is installed with screws (green) on another bracket in the chassis.

Bearingbracket

As already mentioned, the bearinghouses are mounted on additional brackets. Like the motor brackets, these brackets consist of a plate with screw holes () to which end plates are welded

via which the component is installed in the chassis (). The same forces act on this bracket as on the bearinghouse with the weight of the bearinghouse itself ().

Materials

Component	Number	Mass [kg]	Total Mass [kg]	Material
Motor	x1	7	14	
Motorshaft	x1	0.4	0.4	C45 Steel
Bevelgear z=20	x1	3	3	C45 Steel
Bevelgear z=40	x1	9.6	9.6	C45 Steel
Gearshaft Press-fitted	x1	0.3	0.3	C45 Steel
Gearshaft bolted	x1	0.7	0.7	C45 Steel
Shaft Joint	x2	4.1	8.2	C45 Steel
Wheelshaft	x2	0.7	1.4	C45 Steel
Wheel	x2	1.7	3.4	Aluminum 6061
Motorbracket	x1			Aluminum 6061
Motorshaft-bracket and flangebearing	x1			Aluminum 6061
Bearinghouse	x2			Aluminum 6061
Bearingbracket	x2			Aluminum 6061

Table 1.2: Mass and Materials

FEM Results

The result of simulating the motorshaft gives a maximum stress of 120.1 MN/m^2 and thus a safety factor of 5.165 and is therefore stable enough for its area of application.

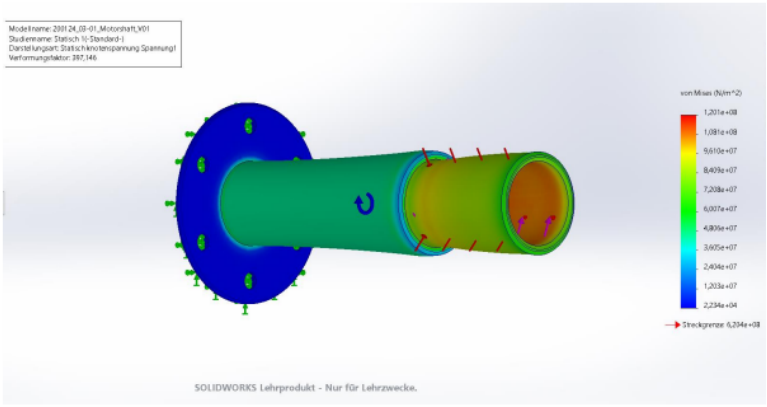

Figure 1.18: Finite Element Method (FEM) simulation results for the Motor shaft

The result of simulating the pressfitted gearshaft gives a maximum stress of $286.1\,\mathrm{MN/m^2}$ and thus a safety factor of 2.027 and is therefore stable enough for its area of application.

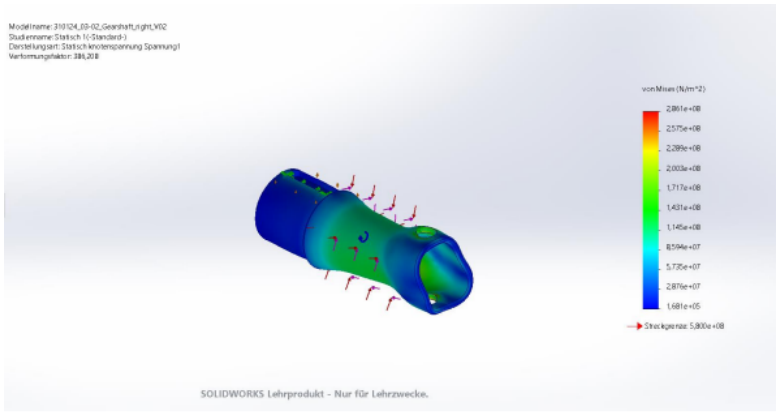

Figure 1.19: Finite Element Method (FEM) simulation results for the pressfitted Gearshaft

The result of simulating the bolted gearshaft gives a maximum stress of $288.1\,\mathrm{MN/m^2}$ and thus a safety factor of 2.013 and is therefore stable enough for its area of application.

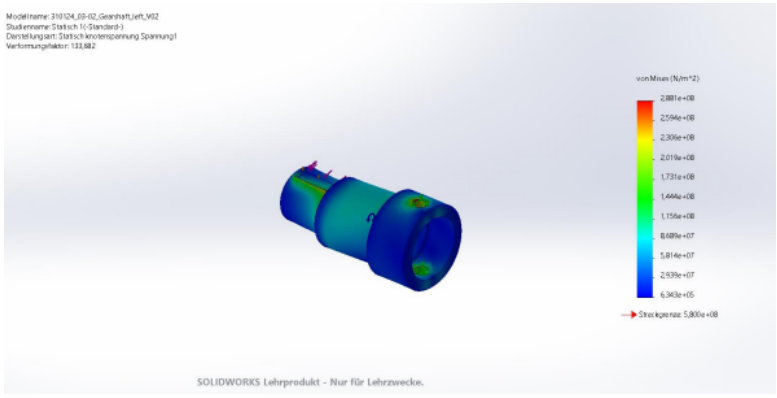

Figure 1.20: Finite Element Method (FEM) simulation results for the bolted Gearshaft

The result of simulating the wheelshaft gives a maximum stress of $284\,\mathrm{MN/m^2}$ and thus a safety factor of 2.042 and is therefore stable enough for its area of application. As this part is identical on both sides of the pod and has to withstand the same forces, we are only showing a single simulation here.

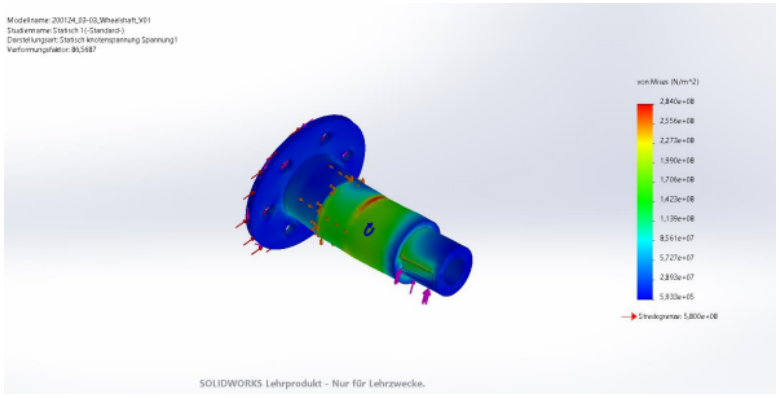

Figure 1.21: Finite Element Method (FEM) simulation results for the wheelshaft

The result of simulating the wheel gives a maximum stress of 19.89 MN/m^2 and while we manufacture this of a Aluminum 6061 compuond, a safety factor of 2.772 and is therefore stable enough for its area of application. As this part is identical on both sides of the pod and has to withstand the same forces, we are only showing a single simulation here.

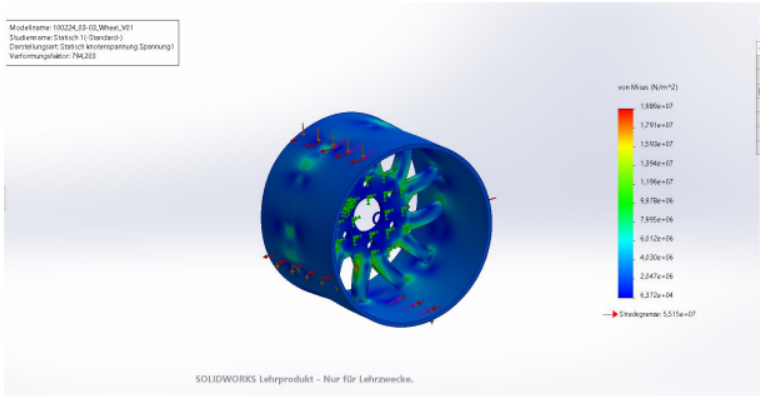

Figure 1.22: Finite Element Method (FEM) simulation results for the wheels

The result of simulating the motorbracket gives a maximum stress of XX N/m^2 and thus a safety factor of XX and is therefore stable enough for its area of application. As this part is identical on both sides of the pod and has to withstand the same forces, we are only showing a single simulation here.

The result of simulating the motorshaftbracket gives a maximum stress of XX N/m^2 and thus a safety factor of XX and is therefore stable enough for its area of application. As this part is identical on both sides of the pod and has to withstand the same forces, we are only showing a single simulation here.

The result of simulating the bearinghouse gives a maximum stress of XX N/m^2 and thus a safety factor of XX and is therefore stable enough for its area of application. As this part is identical on both sides of the pod and has to withstand the same forces, we are only showing a single simulation here. As this part is identical on both sides of the pod and has to withstand the same forces, we are only showing a single simulation here.

The result of simulating the bearingbracket gives a maximum stress of XX N/m^2 and thus a safety factor of XX and is therefore stable enough for its area of application. As this part is identical on both sides of the pod and has to withstand the same forces, we are only showing a single simulation here. As this part is identical on both sides of the pod and has to withstand the same forces, we are only showing a single simulation here.

Mesh and Boundary Conditions

For meshing and specify all required parameters for a successful simulation, we used the standardsettings of Solidworks.

1.2.3 Manufacturing Process

Component	Number	Required procedures
Motorshaft	x1	latheturning, milling
Gearshaft Pressfitted	x1	latheturning, milling, hydraulic pressing
Gearshaft bolted	x1	latheturning, milling
Wheelshaft	x2	latheturning, milling
Wheel	x2	latheturning, milling
Motorbracket	x1	lasercutting
Wheelshaftbracket	x1	lasercutting
Bearinghouse	x2	lasercutting
Bearingbracket	x2	lasercutting, welding

Table 1.3: Components and Manufacturing Details

1.2.4 Integration process

Assembling

Describe how the parts will be assembled, including integration into subordinate structures/systems if applicable.

Assembly interaction

If applicable, describe how the assembly interacts with other assemblies.

1.2.5 Safety considerations

(a) Discuss the safety factor applied to structural elements.
(b) If applicable, discuss the safety factor applied to the demagnetization of permanent mag- nets.
(c) If applicable, discuss high voltage safety considerations for the motor.
(d) Discuss worst-case scenarios (e.g., worst-case braking deceleration) and what you plan to do to avoid or contain them.

1.2.6 FMEA

WILL BE DONE BY PM

Expected Outcomes

Detail the anticipated results from the testing and validation processes.

Risk Mitigation

Discuss the potential risks associated with the system and how they will be mitigated.

Impact Resistance Detail a contingency plan in case the system does not perform as expected.

1.2.7 Testing

Provide a test plan including setup, procedure, and expected outcomes. Outline which factors are critical to success and how they will be validated.

1.2.8 Full-scale adaptation

- Funktioniert wie herkömmliche Eisenbahn - Für die Beschleunigung im Full scale möglich - Sobald der Pod mit levitation anfängt, werden die Reifen angehoben, und das derzeitige propulsion system abgeschaltet

1.2.9 References

EMRAX 188 Technical Data Table

Type / Technical data	EMRAX 188 High Voltage			EMRAX 188 Medium Voltage			EMRAX 188 Low Voltage		
Air cooled = AC Liquid cooled = LC Combined cooled = Air + Liquid cooled = CC	AC	LC	CC	AC	LC	CC	AC	LC	CC
Ingress protection	IP21	IP65	IP21	IP21	IP65	IP21	IP21	IP65	IP21
Cooling medium specification (Air Flow = AF; Inlet Water/glycol Flow = WF; Ambient Air = AA) If inlet WF temperature and/or AA temperature are lower, then continuous power is higher.	AF=20m/s; AA=25°C	WF=8l/min at 50°C; AA=25°C	WF=8l/min at 50°C; AA=25°C	AF=20m/s; AA=25°C	WF=8l/min at 50°C; AA=25°C	WF=8l/min at 50°C; AA=25°C	AF=20m/s; AA=25°C	WF=8l/min at 50°C; AA=25°C	WF=8l/min at 50°C; AA=25°C
Weight [kg]	6,8	7,0	7,0	6,8	7,0	7,0	6,8	7,0	7,0
Diameter ø / width [mm]	188 / 77								
Maximal battery voltage [Vdc] and full load/no load RPM	400 Vdc (6400/7600 RPM)			270 Vdc (6750/7830 RPM)			100 Vdc (7000/7800 RPM)		
Peak motor power at max RPM (few min at cold start / few seconds at hot start) [kW]	**70**								
Continuous motor power (at 3000-6000 RPM) depends on the motor RPM [kW]	**15 - 28**	**15 - 30**	**17 - 35**	**15 - 28**	**15 - 30**	**17 - 35**	**15 - 28**	**15 - 30**	**17 - 35**
Maximal rotation speed [RPM]	**7000 (8500 peak for few seconds)**								
Maximal motor current (for 2 min if cooled as described in Manual) [Arms]	200			300			800		
Continuous motor current [Arms]	100			150			400		
Maximal peak motor torque [Nm]	**100**								
Continuous motor torque [Nm]	**50**								
Torque / motor current [Nm/1Aph rms]	0,60			0,39			0,15		
Maximal temperature of the copper windings in the stator and max. temperature of the magnets [°C]	120								
Motor efficiency [%]	92-98%								
Internal phase resistance at 25 °C [mΩ]	/			/			/		
Input phase wire cross-section [mm²]	10,2			15,2			38		
Wire connection	star								
Induction Ld/Lq [µH]	/			/			/		
Controller / motor signal	sine wave								
AC voltage between two phases [Vrms/1RPM]	0,0384			0,0252			0,00923		
Specific idle speed (no load RPM) [RPM/1Vdc]	19			29			78		
Specific load speed (depends on the controller settings) [RPM/1Vdc]	16 – 19			25 – 29			70 – 78		
Magnetic field weakening (for higher RPM at the same power and lower torque) [%]	up to 100								
Magnetic flux – axial [Vs]	/			/			/		
Temperature sensor in the motor	kty 81/210								
Number of pole pairs	10								
Rotor Inertia (mass dia=160mm, m=3,0kg) [kg*cm²]	/								
Bearings (front:back) - SKF/FAG	6204:6204 (for radial forces) or 6204:7204 (for axial-radial forces; for pull mode; focusing on very high axial load, e.g. for air propeller) or 6204:3204 (for axial-radial forces; for pull-push mode; »O« orientation, α=25°); other bearings are possible (exceptionally)								

www.emrax.com Version 5.1 / August 2018

Figure 1.23: Motor Specifications

1.3 Cooling System

1.3.1 Overview

Requirements and Constraints

The cooling system plays a pivotal role in keeping the motor, battery, and traction controller within safe temperature limits. Overheating can lead to reduced efficiency and potentially shorten the lifespan of these components. For instance, excessive heat could cause bearings to wear out faster, damage motor windings, and even demagnetize permanent magnets. Given the hyperloop's low-pressure environment, we must think beyond standard air cooling methods. Consequently, the exploration of alternative cooling techniques, such as liquid cooling, cooling with the Phase Changing Materials are becoming imperative for ensuring the system's reliability and efficiency.

Estimated Cost and Part List

The total estimated manufacturing cost for the cooling system is approximately 1200 Euros, considering the primary components outlined in the table. Despite its comprehensive functionality, the system maintains a relatively lightweight and compact profile, comprising only a select few components. This cost-effective design approach ensures efficient performance without compromising on reliability or functionality.

Table 1.4

Table 1.4: Components and Manufacturing Details

Component	Number	Mass [kg]	Size [mm]	Material	Manufacturing process	In-house/ Outsourced
Heat Exchanger	x1	1.1	100 x120 x100	Aluminum	LPBF Printing	in-house
Drain Valve	x1	0.02	M8	Aluminum	Latheturning	in-house
PCM	x1.75 [liters]	2	-	PCM	-	outsourced
Deionized Water	x3 [liters]	3	-	Water	-	outsourced
Coolant Pump	x1	1.2	-	-	-	outsourced
Filter	x1	0.1	-	-	-	outsourced
Coolant Temperature Sensor	x2	0.2	-	-	-	outsourced
Surface Temperature Sensor	x3	0.2	-	-	-	outsourced
Flow Meter	x1	0.1	-	-	-	outsourced
Pressure Sensor	x4	0.1	-	-	-	outsourced
Piping	x5 [meters]	0.9	10 x 16	-	-	outsourced
Piping	x2 [meters]	0.4	20 x 26	-	-	outsourced
Tank	x1	0.2	138 x 160	-	-	outsourced
Fittings	x15	-	-	-	-	outsourced

1.3.2 Objectives, Design process, and Cooling Requirements

Figure 1.24

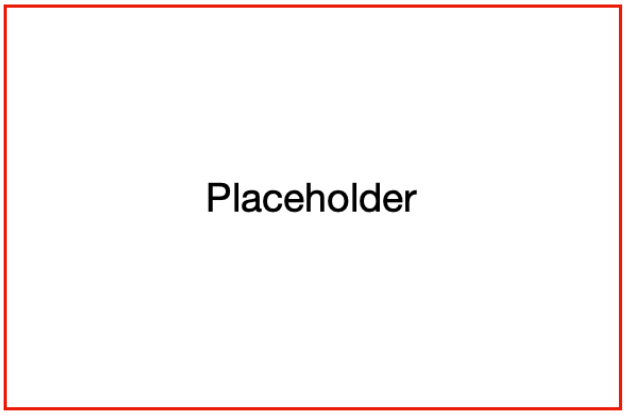

(a) Front view of the pod

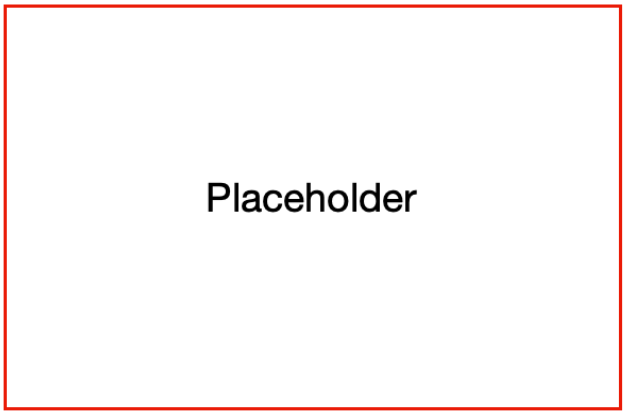

(b) Top view of the pod

Figure 1.24: Placement of the Cooling system

Motor

The EMRAX motor is required to operate within a temperature range of -40□C to 120□C for both the copper windings and magnets. To safeguard against overload, a temperature sensor is integrated into the motor and must be linked to the controller. If the temperature surpasses the permissible limit, the controller adjusts the motor's current output to lower levels until the temperature stabilise within the acceptable range, with a worst-case motor efficiency of 92□, approximately 4.8 kW of heat is generated during operation.

The manufacturer recommends a coolant flow rate of 6 to 8 litres per minute, with the coolant maintained at a maximum temperature of 50□C when entering the motor. Additionally, ambient air temperature surrounding the motor should ideally be 25□C or lower. [Ref - Product Spec Emrax Motor]

Traction Controller

According to the product specification, the maximum permissible temperature for the traction controller is 150□C. However, to guarantee peak performance and longevity, it's essential to maintain temperatures below 90□C. After assessing the operating current and internal resistance, the estimated heat generation was calculated to be 0.56 kW. Through heat transfer calculations from the power module baseplate, equipped with fins, to the coolant, a water flow rate of 0.7 litres per minute was determined necessary to sustain the traction controller's temperature at 90□C.This ensures optimal cooling performance and contributes to the longevity and efficiency of the entire cooling system.

Battery

The battery system within the hyperloop pod generates approximately 3.84 kW of heat during operation. This heat generation is primarily due to internal resistance within the battery cells as electrical energy is converted into usable power. To maintain safe and efficient operation, it is imperative to ensure that the temperature of the battery remains below 75□C.

When a battery operates at elevated temperatures, several detrimental effects may occur. High temperatures can accelerate the degradation of battery components, including the electrolyte and electrode materials, leading to reduced battery capacity and lifespan. Additionally, overheating increases the risk of thermal runaway, a phenomenon where the battery temperature rapidly increases, potentially resulting in fire or explosion.

Cooling Requirements and Strategies

To mitigate these risks and ensure the longevity and safety of the battery system, effective cooling strategies are essential. This includes implementing cooling systems, such as liquid cooling or cooling plates, to dissipate the heat generated by the battery during operation.

To ensure optimal cooling for all three vital components, the system necessitates a total coolant volume of 1 liters of de-ionised water. This calculation factors in the total heat generation (9.2 kW), the duration of a single run at the European Hyperloop Week Competition (20 seconds), and a safety factor of 3 (total time 60 seconds). After 60 seconds of operation, the maximum temperature of the 3 liters of coolant reaches approximately 66.5□C, well below the specified temperature limits. Further analysis during testing phase will provide valuable insights into coolant temperature changes and component temperatures.

To enhance the cooling performance of the cooling System, a refined hardware architecture will be implemented. Temperature levels play a critical role in determining the durability and efficiency of the motor, battery, and traction controller within the hyperloop pod. Elevated temperatures can adversely affect various components, including bearings, motor windings, and permanent magnets, potentially leading to demagnetisation. Therefore, prioritising the enhancement of cooling systems is essential for achieving significant long-term cost savings and improved performance. Given the impracticality of air cooling in the low-pressure hyperloop tube environment, alternative approaches such as liquid cooling and the use of Phase changing materials must be explored.

Hardware Architecture for Enhanced Cooling

As illustrated in figure 1.28, cold water stored at room temperature (approximately 20-25□C) will undergo filtration and then be pumped into the water jackets of the motor, traction controller, and battery in a closed-loop configuration, with a flow rate ranging from 8 to 12 liters per minute. Continuous monitoring of the coolant, motor, traction controller, and battery temperatures will be conducted. Should the temperature of any component exceed the specified limit, the control system will promptly deactivate the pod's drive motor.

Given the absence of heat transfer with the atmosphere during operation, the coolant temperature will gradually increase. Consequently, it's imperative that the coolant within the system remains below the temperature limits of each component. Cooling down the coolant prior to the pod's subsequent operation will be necessary.s Pressure sensors have been strategically positioned at designated locations, as depicted in the diagram, to accurately gauge pressure drops across the water jackets during the testing phase. This data will be instrumental in fine-tuning the system's performance and ensuring optimal cooling efficiency.

1.3.3 Appearance and Integration

Coolant

Deionized water has been selected as the primary coolant for the system due to its low electrical conductivity. This choice is paramount in minimising the potential adverse effects of coolant leaks on the pod's electronic components. Although glycol is a common coolant choice in many cooling systems, it is not utilized in this particular system. This decision is attributed to the fact that the operating temperatures within the system consistently remain well above the freezing point of water, rendering glycol unnecessary.

Coolant Pump

During the testing phase, the Rheinmetall WUP 25 pump will serve as the primary pump for the cooling system. Although typically employed in the realm of combustion engines and vehicle climate control systems, the WUP 25 pump demonstrates versatility by effectively handling various cooling tasks, including cooling DC/DC converters, batteries, electric motors, and power electronics. Its compact design allows for installation in constrained spaces, and it offers a range of hydraulic and electrical interfaces to suit diverse applications. Equipped with a control and diagnostic pin, the WUP 25 pump facilitates speed control via a PWM input signal [Ref = Product Data Sheet WUP 25].

To ensure optimal performance, the pump will be mounted at a mid-level position within the cooling circuit. This strategic placement helps prevent the formation of air traps (if mounted at the highest position) and minimizes the risk of debris accumulation within the pump (if mounted at the lowest position) [Ref = Product Data Sheet WUP 25]. However, due to the current uncertainty regarding the pressure drop in the system, it may be necessary to explore alternative pump options or implement a multi-stage pump system (in series) alongside the existing model. The exact pressure drop across the water jackets will be determined through rigorous testing

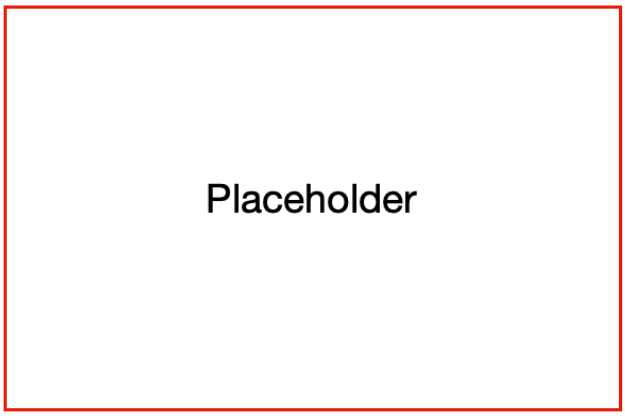

Figure 1.25: Coolant pump

Coolant Storage Tank

The cooling system is designed with consideration for the realistic scenario of the pod traveling through a low-pressure tube (near vacuum), limiting heat exchange with the atmosphere. The coolant in the circuit absorbs heat from the motor, battery, and traction controller, causing an increase in coolant temperature over time. The current design ensures sufficient coolant storage to keep all components well below the required maximum operating temperature.

For the hyperloop pod slated for participation in the European Hyperloop Week, a typical vehicle coolant tank with a capacity of 1 liter has been deemed adequate. This capacity aligns with the demands of the pod's cooling requirements, guaranteeing optimal performance throughout its operation.

Water Jackets

The water jacket for the motor will be provided by the motor manufacturer, ensuring compatibility and optimal performance. For the water jackets of the traction controller and battery, custom fabrication will be undertaken based on the recommendations provided by their respective manufacturers. This approach guarantees that each component receives tailored cooling solutions to meet its specific requirements and operating conditions.

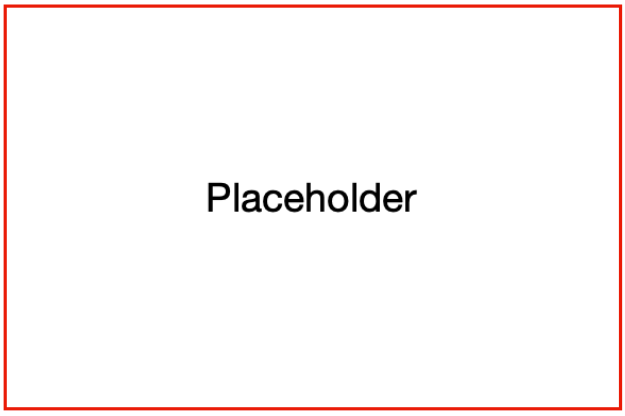

Figure 1.26: Coolant tank

Piping

Two piping options are under consideration. i) CPVC pipes, chosen for their resistance to high temperatures, scaling, durability, low cost, and ease of installation. The specific piping route is yet to be finalized , but the total length is estimated to be around 6 meters. ii) The potential use of soft tubing is also being explored.

1.3.4 Heat Exchanger

Role and Benefits in the cooling System

In the context of the cooling system described for the hyperloop pod, a heat exchanger would play a crucial role in transferring heat between the coolant circulating within the closed-loop system and the surrounding environment. As the coolant circulates through the system, it absorbs heat from the motor, battery, and traction controller, thereby increasing in temperature. Since the hyperloop pod operates in a low-pressure tube with limited heat exchange with the atmosphere, the heat exchanger facilitates the dissipation of heat even in this constrained environment.

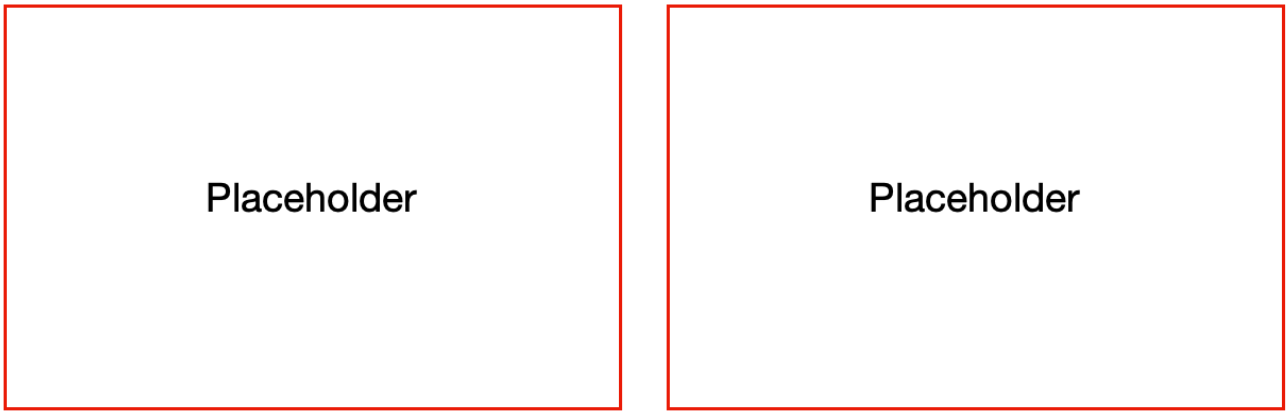

(a) Closed View (b) Open View

Figure 1.27: Gyroid Heat Exchanger

Use of Phase Change Materials (PCMs)

Introducing the heat exchanger utilizing phase change materials (PCMs) into the cooling system for the hyperloop pod would offer several advantages and could enhance its performance in specific

scenarios, incorporating a heat exchanger with the use of phase changing material serves several important purposes:

- Enhanced Heat Absorption and Release: The PCM, such as stearic acid, can absorb and release a significant amount of heat during its phase transition from solid to liquid and vice versa. Integrating a heat exchanger with PCM allows for efficient absorption of excess heat generated by components like the motor, traction controller, and battery.
- Temperature Regulation: By absorbing excess heat from critical components, the heat exchanger helps regulate their temperatures within the specified operating ranges. This prevents overheating, which can lead to performance degradation or damage to components.
- Thermal Energy Storage: The PCM's ability to store thermal energy during its phase change enables the system to store heat when temperatures are within acceptable limits and release it when needed to maintain optimal operating conditions. This helps in managing transient heat loads and stabilizing temperatures over time.
- Reduced Coolant Temperature: By utilizing the PCM's heat absorption capacity, the heat exchanger can lower the temperature of the coolant circulating in the system. This ensures that the coolant remains within acceptable temperature limits, contributing to the overall effectiveness of the cooling system.
- Increased Efficiency: Integrating a heat exchanger with PCM can improve the overall efficiency of the cooling system by maximizing heat transfer capabilities and reducing the reliance on conventional cooling methods alone.
- Extended Operating Time: The thermal energy stored in the PCM can be utilized to extend the operating time of the system before coolant temperature rises beyond acceptable levels. This can be particularly beneficial during transient operating conditions or in the event of temporary power interruptions.

Overall, incorporating a heat exchanger with the use of phase changing material adds an additional layer of heat management capability to your cooling system, contributing to improved performance, efficiency, and reliability in the hyperloop pod environment.

Stearic Acid

Stearic acid stands out as a highly versatile phase change material (PCM) deployed across diverse applications. Its unique characteristic of transitioning from solid to liquid state at a precise temperature renders it exceptionally suitable for thermal energy storage purposes. Through this phase transition, stearic acid exhibits remarkable heat absorption and release capabilities, making it a valuable asset in scenarios demanding efficient temperature regulation and thermal energy management. Commonly found in applications ranging from building insulation to specialized temperature control systems, stearic acid's efficacy as a PCM underscores its widespread industrial utility.

Stearic Acid Stearic acid is a saturated fatty acid with the chemical formula $C_{18}H_{36}O_2$. It is a long-chain carboxylic acid, meaning it has 18 carbon atoms in its hydrocarbon chain and a carboxyl group (COOH) at one end. Here are some key properties and uses of stearic acid:

Physical Properties:

- Melting Point: Stearic acid is a solid at room temperature and has a melting point of around $69 - 70$ degrees Celsius ($156 - 158$ degrees Fahrenheit).
- Appearance: It is a white, waxy solid with a characteristic fatty odor.

Chemical Properties:

- Structure: Stearic acid has a straight-chain structure with 18 carbon atoms, making it a saturated fatty acid. Hydrophobic: Like other fatty acids, stearic acid is hydrophobic, meaning it repels water.

In summary, stearic acid is a versatile compound with various industrial applications, and its phase change properties make it useful in thermal energy storage applications as well.

1.3.5 Calculations and Simulations

WILL BE ADDED SOON (Dino)

1.3.6 Safety Measures

Given the close integration of the cooling system with the electronic systems, the primary risk is a coolant leak that could potentially damage electronic components. Preventive measures are outlined in the table below, and deionised water is chosen as the preferred coolant due to its low conductivity.

Potential Failure Modes and Risk Mitigation-

- Coolant Leaks
  - Effect of Failure: Damage Electronic components
  - Root Cause: Poor sealing at pipe joints
  - Risk Mitigation Strategy: Maintain the correct coolant level, avoid overfilling the tank, sealing pipes with hose clamps and use deionized water as a coolant.
- Temperature of Critical component rises above rated temperature
  - Effect of Failure: Damage Component
  - Root Cause: Insufficient cooling due to prolonged operation
  - Risk Mitigation Strategy: Implement a control system to halt the motor and by installing two temperature sensors if temperatures exceed prescribed limits for the motor, battery, or traction controller.
- Temperature of Critical component rises above rated temperature
  - Effect of Failure: Coolant Leaks
  - Root Cause: Insufficient cooling due to air traps or exceeding defined operation time
  - Risk Mitigation Strategy: Position of the system including heat exchanger is placed at the front of the pod, in order to purge air after refilling, and adhere to defined operation times.
- Blocks in piping
  - Effect of Failure: Insufficient cooling and damage to components
  - Root Cause: Foreign particles/debris
  - Risk Mitigation Strategy: Introduce filters in the piping system and conduct regular cleaning maintenance.

FMEA analysis

References

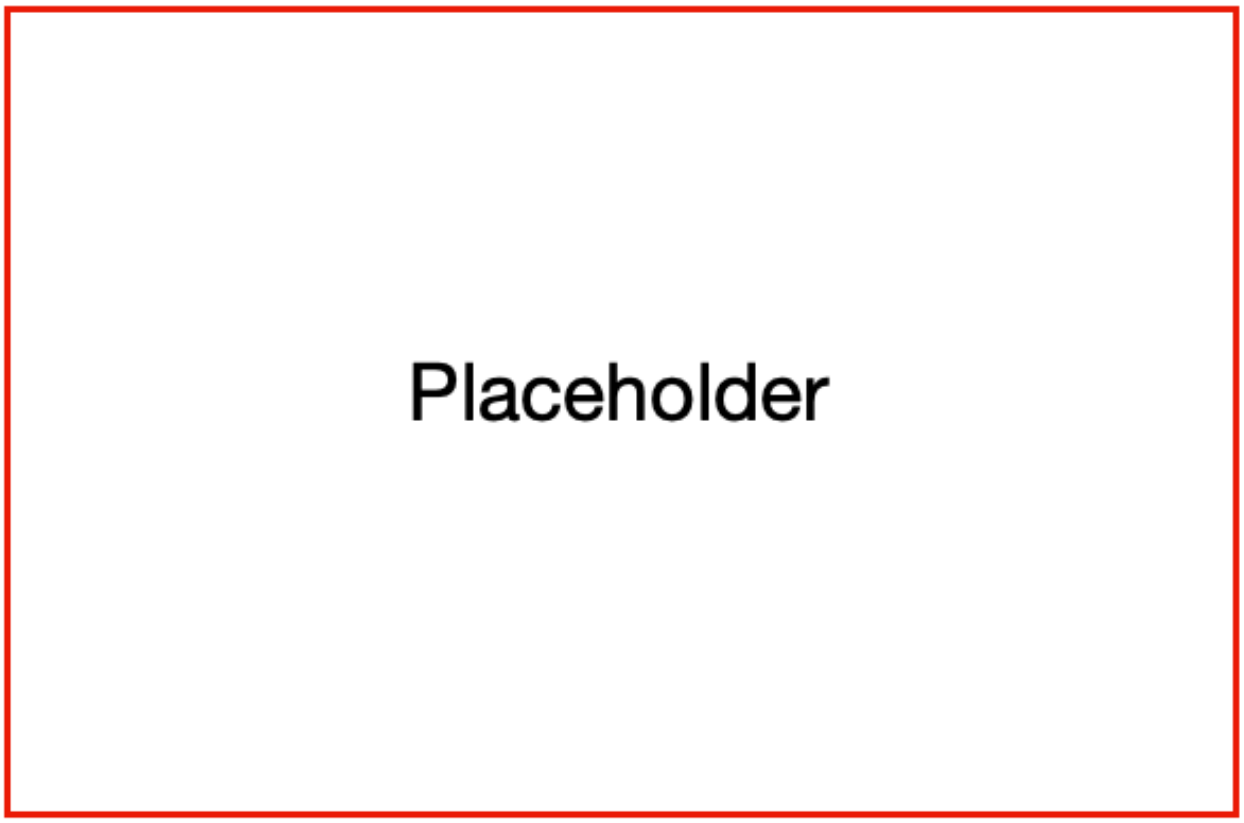

Figure 1.28: Flowchart of the system

Electrical Systems

Take a short look at the whole text before starting to write your part.

2.1 Introduction

2.1.1 (b) List of all discrete electrical subsystems.

We are implementing the following subsystems:

- LV Battery
- HV Power Supply, including
  - Battery Management System
  - Insulation Monitoring Device
- Traction Inverter
- Propulsion Motor
- Sense and Control System

2.1.2 (a) Brief overview with the main points of the HV and LV systems.

Our electrical system provides the electrical power for the propulsion and control systems. We have a low voltage circuit nominally rated at 24V (for control systems) and a high voltage level circuit at 444V (for the traction system). The low voltage circuit activates and controls the high voltage power supply through the Battery Management System and is hence designed for reliability.
The high voltage circuit is designed for safety, being potentially lethal, and power, in order to maximize the use of the motor. An OEM Insulation Monitoring Device checks for the (lack of) resistance between chassis and the HV power line in case of short circuits.
The traction inverter uses the electric power of the high voltage battery to power the motor, converting DC power into AC phases. We use an OEM device that is used in automotive purposes.

The motor is a lightweight motor from Emrax. Even though it belongs to the traction system, we will document it in the electrical section, as the development team of the originally planned inhouse-built inverter took over the duty of the electrical part of the motor system, too.

The Sense and Control System is not part of the EHW definition of the electrical systems. Since we have to provide a documentation nonetheless and the team designing the electrical subsystem also designed the Sense and Control system, we decided to include it as a part of the electrical

subsystem documentation. It controls the brakes, the thermal pump, the telemetry line and the telemetry unit, as well as additional physical sensors.

Our general design of this season is inspired by conventional modes of transportation, as we have not had the capacity to start developing a levitation system by this season Thus, we focussed on an electrical system that drives our friction-based motor with excelling acceleration, which is a problem that railway systems frequently face.

In between design and production phase, we received a sponsorship of Leadrive, a local startup for research on automotive power electronics. Furthermore, the institute for electrical systems (ISEA) of our home university offered us assistance in the production of battery cells. Therefore, our workload was eased, which turned out to be favorable because of our lack of team members in the electrical field. This has been a crucial constraint in the design and planning process of the electrical department since the last season. Only shortly before submitting the ITD, we were able to make an estimation of realistic goals for the new team.

This year, we would like to set the path for magnetic levitation in the future, relying on an active system inside the vehicles. This was taken into consideration when designing the power dimensions, keeping plenty of overhead for the future, which aligns with our goal of sustainability. By having reusable modules, the design process of the upcoming years will be simplified.

We collaborate with the following institutions for support in the electrical department (including S&C):

- Altium: Sponsored Licenses of PCB design software
- Festo: Sponsored mechanical components and sensors for pneumatic systems.
- Mouser Electronics: Sponsored certain electronics.
- Würth Elektronik: Sponsored certain electronics.
- Leadrive: Sponsored traction inverter
- Vector Informatik: Sponsored CANoe Suite, including technical training for CAN networks.
- Bender: Sponsored Insulation Monitoring Device.
- ISEA: Assembling our battery pack.

2.1.3 (c) Wiring diagram of the HV system.

To Sourajit.

2.2 LV Battery

2.2.1 Overview

(a) Explain the main requirements and constraints that drive the design.
Strict EHW rules
reliability
reusability
lightweight
power of pump, valves etc.

Our Low Voltage system drives all electrical and digital control systems of the Fermion. As stated previously, reliability is crucial in this case. A failure of any component may lead to the

shutdown of critical systems, such as the battery management system. Furthermore, an overvoltage may potentially damage these systems, causing safety hazards. We had the option between building a LV battery pack from spare LiPo cells we ordered for the HV battery pack, and using automotive-grade ventilated lead-acid batteries. After considering the safety problems of LiPo cells and the efforts of either building a second (smaller) LV BMS or taking the risk of having a singular point of failure by controlling both systems with the same BMS, powering the BMS with the cells it controls, we went for the approach with lead-acid batteries, that is widely used in automotive systems. It is regarded as more reliable and robust compared to the Lithium-Ion pendants that we use for the High Voltage System.

Power requirements

We consider the power consumption of all components in the low voltage power line for the power requirements:

(Moussa: Bitte finde die einzelnen Daten heraus. Pumpe ist Pierburg CW150A. Valve ist bei den brakes controllern. Raspberry Pi und Microcontroller passen.)

- Solenoid Valves: According to the data sheet, the valves use 2.25 Watts à 4 valves = 9 Watts. While switching, which takes 3.5 ms, they use 8.5 Watts. Assuming that we switch all four valves 20 times, we have an additional consumption of $0.595J$, which is almost negleglible. We will assume a power consumption of 10 Watts for tolerance.
- Thermal Pump: Given the water flow rate, we calculated a theoretical need of 34 Watts for the pump. As we do not have experimental data, we assume that 50 Watts are required at maximum.
- Raspberry Pi 4: One Raspberry Pi 4B consumes 10 Watts.
- Raspberry Pico W:
- One Raspberry Pico W does not consume more than 1 Watt.
- Microcontrollers (TIC2000 F280039C):
  - According to datasheet, one microcontroller uses $3.3V * 0.11A = 0.363W$. The controller circuits will not exceed 5 Watts in total.
- BMS (Orion BMS 2, 180 Cells): Our BMS consumes up to 2 Watts, according to the datasheet.
- Leadrive Inverter: Using the nominal power ratings of 3 A at 24 V, we have a power consumption of 72 Watts.
- IMD: Our IMD consumes up to 2 Watts, according to the datasheet.
- Network transceiver: We use the Rocket M2, which consumes up to 6 Watt of energy, according to the datasheet.
- Precharge relay and contactors: Our precharge relay uses $0.32W$, our main contactors use $2 * 12V * 1A$ in total. We will calculate with 25W.

Now, summing up all the power requirements, we have $10W + 50W + 10W + 1W + 5W + 2W + 72W + 2W + 6W + 25W = 183W$, which is roughly 7.7 A at 24V.
Using the discharge chart of the data sheet of the LV Battery,

it is evident that even at full power (9A - including some headroom for losses), we can run our low voltage system for 20 minutes. During the competition, we can rule out that we will use that much power over the whole 20 minutes. Assuming that the pump is activated while the HV system is at work, and that this duration takes 2 minutes maximum (the actual run will be much less - max. 20 seconds), and we assume only a usage of 111 W for the rest of the time, we can use the LV battery for well over 20 minutes.
In conclusion, the capacity of 9Ah is a trade-off between the mass and the available runtime of the system.

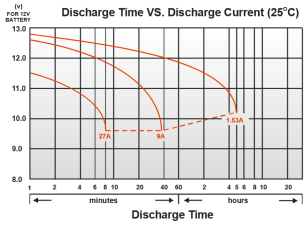

Figure 2.1: Discharge chart of LV battery cell

2.2.2 Electrical and mechanical design process

Schematic

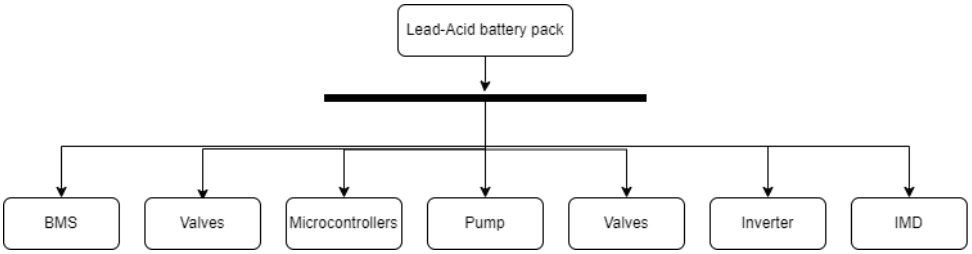

Figure 2.2: Diagram of LV connections

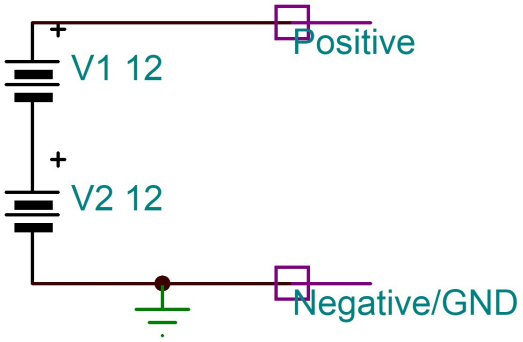

Figure 2.3: Schematic of LV battery cell

(b) Present temperature simulations for vacuum conditions.

We did a rough estimation based on the internal resistance of the battery, which is around 0.014Ω according to the datasheet. We will assume 0.02Ω. Using the equation of heat loss, we get $P = I^2 * R = 8^2 * 0.02 * W = 1.28W$.
The ... Bohdan

For our heat simulations, we used the software of ANSYS. By vacuum conditions, we assumed the lack of gas flow, which eliminates the cooling heat flow from winds. The simulation tool solves

the heat transfer equation $\frac{\partial T}{\partial t} = \alpha \left(\frac{\partial^2 T}{\partial x^2} + \frac{\partial^2 T}{\partial y^2} + \frac{\partial^2 T}{\partial z^2} \right)$ by discretizing through Finite-Element-Methods.

2.2.3 Electrical system characteristics

Battery Type	Lead-Acid(integrated)
Capacity[Ah]	9
Nominal Voltage[V]	12
Cell configuration	2s
Max. discharge [A]	10
Weight per cell [Kg]	2,7
Dimensions per cell (L x W x H)[mm]	151 x 65 x 94

Table 2.1: LV battery cell characteristics

Battery Type	Lead-Acid(integrated)
Capacity[Ah]	9
Nominal Voltage[V]	24
Cell configuration	2s
Max. discharge [A]	10
Weight [Kg]	5.5
Dimensions (L x W x H)[mm]	151 x 65 x 94

Table 2.2: LV battery pack characteristics

2.2.4 Interface with other system

Briefly reference the communication protocols or control mechanisms of the boards, which should be explained in the respective Sense and Control subsection.
All the electric subsystems are located within the pod.

It powers the entire sensing, control and telemetry system. The LV battery itself does not communicate. Its sensor data is processed by the thermal control board. When the voltage drops below a certain threshold, the complete system shuts down.

2.2.5 Final system description

The two lead-acid batteries, chained in series, provide a nominal voltage of 24V (12V each). When fully charged, the voltage can increase to up to 26V. The lead acid batteries have the problem of voltage drops while discharging. Hence, we monitor the voltage while using the LV battery system. Furthermore, we monitor the temperature through a thermistor to prevent usage under overtemperature .

The 24 V power source gets transferred down to 12V (for the Thermal Pump) and 5V for the micro-controllers by buck converters, and drives the valves and several sensors at 24V simultaneously. It is being monitored by NTC thermistors for overheating, and by the thermal system for undervoltage.
After reaching out to the EHW technical committee, we were able to clarify that a BMS, used by Lithium-Ion batteries, is not required for lead-acid batteries due to the inherently different chemical structure which makes over- and undercharging much less critical.

For charging, we are using a battery charger specified for 12V and 24V lead acid cells from Würth 0510955908. The charging of lead-acid batteries in series is unproblematic, given that we regularly test for drifts and manually balance the cells.

2.2.6 Manufacturing process

As the cells come in hard-shell covers already, the manufacturing process is not very complicated. We will 3D-print a casing.

2.2.7 Testing

We will test whether the lead acid cells and the thermistors are accurate to their datasheet.

2.3 High Voltage Power Supply

2.3.1 Overview

(a) Explain the main requirements and constraints that drive the design.

2.3.2 Electrical and mechanical design process

(a) Present Schematics or logic diagrams of the boards.

(b) Present temperature simulations for vacuum conditions.

For our heat simulations, we used the software of ANSYS. By vacuum conditions, we assumed the lack of gas flow, which eliminates the cooling heat flow from winds. The simulation tool solves the heat transfer equation $\frac{\partial T}{\partial t} = \alpha \left(\frac{\partial^2 T}{\partial x^2} + \frac{\partial^2 T}{\partial y^2} + \frac{\partial^2 T}{\partial z^2} \right)$ by discretizing through Finite-Element-Methods.

From | To	LV Battery	HV Battery	BMS	Traction Inverter	Motor	Cooling System
LV Battery	-	-	Powers	Powers control system	-	Powers pump and control system
HV Battery	-	-	Connects to	Provides power	-	-
BMS	-	-	Controls	-	-	-
Traction Inverter	-	-	-	-	Propels	X
Motor	-	-	-	-	-	-
Cooling System	-	-	-	Cooling	Cooling	Cooling (implicitly)

Table 2.3: Physical connection matrix

From \ To	LV Battery	HV Battery	BMS	Traction Inverter	Motor	Cooling System	Brakes Controller	Telemetry Unit
LV Battery	-	-	-	-	-	-	-	-
HV Battery	-	-	Discharge rate, voltage level	-	-	-	-	-
BMS	controls	controls	-	-	-	-	-	sends data
Traction Inverter	-	-	-	-	-	-	-	sends data
Motor	-	-	-	-	-	-	-	-
Cooling System	-	-	-	-	-	-	-	sends data
Brakes Controller	-	-	-	-	-	-	-	sends data
Telemetry Unit	-	-	updates limits	sends commands	-	sends target rates	sends commands	-

Table 2.4: Data connection matrix

2.3.3 Description of subsystem control

(a) Briefly reference the control systems of the boards, which should be explained in the levitation or propulsion subsection respectively.

We configure the BMS prior to the competition.

2.3.4 Electrical system characteristics

2.3.5 Interface with other system

(a) Briefly reference the communication protocols or control mechanisms of the boards, which should be explained in the respective Sense and Control subsection.
All the electric subsystems are located within the pod.

The phsyical connection matrix is as following:

The data connection matrix is as following. All communication between boards are via CAN, if not specified otherwise:

2.3.6 Final system description

Battery Cells

High Voltage Network:

Our high voltage battery will make use of lithium-ion polymer technology. We use 120 pouch-format cells from Shenzhen GrePow Battery Co. Ltd rated at 45C maximum discharge that we plan to connect in series. The finished package (main battery pack) will be assembled by the team. We are going to connect the 120 cells connected in series and that will have 1 parallel line. This will roughly have 504 Volt at max (using $120 * 4.2V = 504V$) which provides sufficient electricity to power the motor. The battery pack will provide up to 350 Amps of DC current available to the inverter. However, neither the inverter nor the motor is not rated for such high currents nominally.

Therefore, the maximum output current of the HV Battery will be rated at 200 A maximum (peak) and 100 A continuous.

We will stack 30 cells in series per pack and then stack 4 of them to get the full battery pack. No we won't.

BMS

Our battery management system

The Orion BMS 2, connected to the HV battery, protects it and improves its life, efficiency. Operational Mechanics

The Orion BMS 2 facilitates real-time monitoring and management of each cell within the HV battery pack, which consists of 120 lithium-ion polymer cells arranged in a series configuration to achieve a nominal voltage of 504V. This arrangement necessitates precise control and monitoring to prevent overcharging, deep discharging, and to ensure balanced cell voltages, all of which are within the Orion BMS 2's capabilities.

1. Cell Voltage Monitoring and Balancing: The BMS continuously monitors the voltage of each cell, ensuring that all cells operate within their safe voltage range. Cell balancing is performed to equalize the charge across all cells, thereby enhancing the battery pack's overall efficiency and lifespan.
2. Temperature Monitoring: Given the high energy density of the HV battery pack, thermal management is paramount. The Orion BMS 2 monitors the temperature of individual cells and the battery pack as a whole, activating cooling measures when necessary and preventing operation under extreme temperatures that could damage the battery or compromise safety. The Orion BMS 2 itself tracks the temperature of 8 individual cells. 28 other cells are measured by the Thermal Controller.
3. State of Charge (SoC) and State of Health (SoH) Estimation: SoC and SoH estimations are important for optimal battery utilization and health maintenance. The Orion BMS 2 employs advanced algorithms to provide these estimates, ensuring that the battery's capacity is used efficiently.

The integration of the Orion BMS 2 encompasses several safety mechanisms designed to protect the battery pack, the hyperloop pod, and its occupants:

1. Overcurrent and Short Circuit Protection: By monitoring the current flowing in and out of the battery pack, the Orion BMS 2 can detect overcurrent conditions and short circuits, initiating immediate shutdown procedures to prevent damage and ensure safety.
2. High and Low Voltage Protection: The BMS prevents the battery from exceeding its maximum voltage during charging and dropping below its minimum voltage during discharge, thereby avoiding scenarios that could lead to reduced battery life or safety hazards.
3. Thermal Runaway Prevention: Through its temperature monitoring capabilities, the Orion BMS 2 can detect the onset of thermal runaway—a dangerous condition where one cell's failure can lead to a cascading failure of adjacent cells—and take corrective actions to isolate the problem and mitigate potential damage.

Efficiency Enhancements

By optimizing the operational parameters of the HV battery pack, the Orion BMS 2 contributes significantly to the efficiency and performance of the hyperloop prototype:

1. Energy Optimization: By ensuring that all cells are balanced and operate within their optimal voltage and temperature ranges, the BMS maximizes the energy extracted from the battery pack, contributing to the hyperloop's range and speed capabilities.
2. Lifecycle Extension: Through diligent monitoring and management, the Orion BMS 2 extends the useful life of the HV battery pack, reducing the environmental impact and operational

costs associated with battery replacement.

3. □□Predictive Maintenance:□□ By providing detailed data on the SoC and SoH, the Orion BMS 2 enables predictive maintenance, allowing for timely interventions that prevent unscheduled downtimes and extend the battery's lifespan.

Conclusion

The integration of the Orion BMS 2 with the HV battery pack in our hyperloop prototype represents a critical step towards ensuring the system's safety, efficiency, and reliability. Through its comprehensive monitoring and management capabilities, the Orion BMS 2 ensures that the HV battery pack operates within its optimal parameters, significantly contributing to the prototype's overall performance and safety profile. As we progress towards the final stages of the FDD, the detailed exploration of the Orion BMS 2's functionalities underscores our commitment to leveraging advanced technologies for the enhancement of hyperloop transportation systems.

Insulation Monitoring Device

The Insulation Monitoring Device that is mandatory for EHW participants, as well as Formula Students teams, is not built inhouse, after receiving the respective advice from the EHW technical jury. By reaching out to Bender, we received their device through their Formula Students policy. It is configured for ...

2.3.7 Manufacturing process

Our PCB Design

PCBs

Prototyping: Prototype PCBs are fabricated in the FabLab associated with our university. The FabLab provides access to PCB manufacturing equipment and materials, enabling the rapid production of prototypes for initial testing and design validation. Once the PCBs are fabricated, they are assembled manually by our team members. Bigger PCBs are assembled in the facilities of the FabLab with the manual Pick and Place Machine and a reflow oven.

Production: We ordered our final PCBs from JLCPCB, a leading PCB manufacturing service. In addition to JLCPCB, we also collaborate with Würth Elektronik who produce PCBs in Germany, aligning with our goal of sustainability.

Batteries

The production of the low voltage battery pack is rather easy. We will use a 3d printer to print the casing We produced the battery packs in cooperation with the ISEA (Institute for Power Electronics and Electrical Drives) at RWTH, whose experience helped us to assemble and design the parts more efficienciently and more safely, as we had a considerable high voltage system. The casing will consist of polycarbonate. Polycarbonate is a material that is durable , lightweight, and impact resistant. The problems with material degradation through UV emissions does not impact us substantially, as we cover the battery pack inside the shell for most of the time. We will have safety measures preventing too much exposure to UV radiation. Also, the degradation is mainly of cosmetic nature (https://link.springer.com/article/10.1007/s11668-020-01002-9) .

2.3.8 Testing

We started testing software.

2.4 Power Electronics

2.4.1 Overview

Main requirements and design constraints

Our general design of this season is inspired by conventional modes of transportation, as we have not had the capacity to start developing a levitation system by this season Thus, we focussed on an electrical system that drives our friction-based motor with a high amount of acceleration, which is a problem that railway systems frequently face.

In between design and production phase, we received a sponsorship of Leadrive, a local startup for research on automotive power electronics. Therefore, our workload was eased, which turned out to be favorable because of our lack of team members in the electrical field. This has been a crucial constraint in the design and planning process of the electrical department since the last season. Only shortly before submitting the ITD, we were able to make an estimation of realistic goals for the new team.

This year, we would like to set the path for magnetic levitation in the future, relying on an active system inside the vehicles. This was taken into consideration when designing the power dimensions, keeping plenty of overhead for the future, which aligns with our goal of sustainability. By having reusable modules, the design process of the upcoming years will be simplified.

2.4.2 Electrical and mechanical design process

Our initial goal was to design our own traction inverter system, both the control and power stages. After receiving the sponsorship with Leadrive, who also sponsors another student team in Aachen that we collaborate closely with, we decide to put our own, limited sources to other projects temporarily.
This means that we have a automotive inverter, with slightly overdimensioned specifications, to work with. The DC link capacitor of the inverter is charged externally.
The precharge circuit was based on an economic decision. Our pod is not made for a commercial purpose. Thus, fast pre-/discharge times are not highly prioritized. We designed with several different precharge resistors at levels from 50 Ohm to 10 kOhm, and simulated them. The results showed that the low-resistance circuits need very high-power components, which will dissipate a lot of heat and be a potential safety danger. However, we wanted to keep the charging times within reasonable times (<5 seconds).
We simulated a test case with charging the capacitor to a stage where 99.5 □ is charged. Thus, the current flow when the main power line is switched on is well under 100A, which is the continuous rating of our system.
Finally, we chose a resistor with a lot of headroom: We used 3k resistor with a 50 Watt maximum rating.
This gives us the following specifications of our precharge circuit:

- Time Constant (τ):

$$\tau = R \times C = 3000\,\Omega \times 0.24 \times 10^{-3}\,\mathrm{F} = 0.72\,\mathrm{s}$$

- □□Voltage across the capacitor at $t = 5$ seconds□□:

$$V(5) = 500 \times \left(1 - e^{-\frac{5}{0.72}}\right) = 499.52V$$

- □□Rate of Charge at $t = 5$ seconds□□:

$$\left.\frac{dQ}{dt}\right|_{t=5} = C \times \left.\frac{dV(t)}{dt}\right|_{t=5} = 0.24 \times 10^{-3}\,\text{F} \times \frac{500}{0.72} \times e^{-\frac{5}{0.72}}$$

Now, we'll compute the numerical value for $\frac{dQ}{dt}$ at $t = 5$ seconds:

$$\left.\frac{dQ}{dt}\right|_{t=5} = 0.24 \times 10^{-3} \times \frac{500}{0.72} \times e^{-\frac{5}{0.72}} \approx 0.24 \times 10^{-3} \times 694.44 \times e^{-6.94}$$

$$\left.\frac{dQ}{dt}\right|_{t=5} \approx 0.16176\,\text{mA}$$

So, the rate of charge after 5 seconds is approximately 0.16176 mA. The power when switching to the main circuit is, thus, $500V * 0.16176mA = 0.081W$.
We can accept this. Furthermore, our simulations show that the maximum power will not exceed 22 W, whilst the main peak (>5W) lasts less than 2 seconds. The heat

(a) Present Schematics or logic diagrams of the boards.

(b) Present temperature simulations for vacuum conditions.

For our heat simulations, we used the software of ANSYS. By vacuum conditions, we assumed the lack of gas flow, which eliminates the cooling heat flow from winds. The simulation tool solves the heat transfer equation $\frac{\partial T}{\partial t} = \alpha\left(\frac{\partial^2 T}{\partial x^2} + \frac{\partial^2 T}{\partial y^2} + \frac{\partial^2 T}{\partial z^2}\right)$ by discretizing through Finite-Element-Methods.

2.4.3 Description of subsystem control

(a) Briefly reference the control systems of the boards, which should be explained in the levitation or propulsion subsection respectively.

We configure the BMS prior to the competition.

From | To	LV Battery	HV Battery	BMS	Traction Inverter	Motor	Cooling System
LV Battery	-	-	Powers	Powers control system	-	Powers pump and control system
HV Battery	-	-	Connects to	Provides power	-	-
BMS	-	-	Controls	-	-	-
Traction Inverter	-	-	-	-	Propels	X
Motor	-	-	-	-	-	-
Cooling System	-	-	-	Cooling	Cooling	Cooling (implicitly)

Table 2.6: Physical connection matrix

2.4.4 Electrical system characteristics

Parameter	MIN	NOM	MAX	Unit	Conditions
Ambient Temp. for Operation (T_{AMB})	-40	-	90	□C	-
Ambient Temp. for Storage (T_{STO})	-40	-	85	□C	-
Relative Humidity	0	-	95	□	-
Flow Rate of Coolant (V_{CLNT})	8	12	16	l/min	Derating @ $8 \sim 12$ l/min
Inlet Temp. of Coolant (T_{CLNT})	-40	-	85	□C	Derating @ $65 \sim 85$□C
Cooling Inlet Pressure (P_{INLET})	-	-	2.5	bar	-
Pressure Drop between Cooling Inlet and Outlet (P_{DROP})	-	0.25	-	bar	$T_{CLNT} = 65$□$C, V_{CLNT} = 12$ l/min
Input Voltage (V_{DC})	260	600	850	V	Full operation @ $450 - 800$V
Input Current (I_{DC})	-	200	-	A	Continuous
Peak Input Current (I_{DCPK})	-	300	-	A	For max t_{PK} duration
Output Voltage (V_{AC})	-	400	-	Vrms	-
Output Current (I_{AC})	-	-	200	Arms	Continuous
Peak Output Current (I_{ACPK})	-	-	300	Arms	For max t_{PK} duration
Output Power (S_{AC})	-	135	-	kVA	Continuous
Peak Output Power (S_{ACPK})	-	200	-	-	For max t_{PK} duration
Peak Duration (t_{PK})	-	-	60	s	-
Input Voltage for Control (V_{BAT})	6	-	36	V	Full functional @ $8 - 32$V (control board)
Max. Efficiency (η)	97	-	-	□	-
Torque Control Accuracy (ϵ_{TRQ})	-	-	3	□	Torque > 100Nm
	-	-	3	Nm	Torque < 100Nm
Torque Control Speed (t_{TRQ})	-	-	100	ms	-
Speed Control Accuracy (ϵ_{SPD})	-	-	30	rpm	-

Table 2.5: 800V Single Inverter Specifications

2.4.5 Interface with other system

(a) Briefly reference the communication protocols or control mechanisms of the boards, which should be explained in the respective Sense and Control subsection.
All the electric subsystems are located within the pod.

The phsyical connection matrix is as following:

The data connection matrix is as following. All communication between boards are via CAN, if not specified otherwise:

From \ To	LV Battery	HV Battery	BMS	Traction Inverter	Motor	Cooling System	Brakes Controller	Telemetry Unit
LV Battery	-	-	-	-	-	-	-	-
HV Battery	-	-	Discharge rate, voltage level	-	-	-	-	-
BMS	controls	controls	-	-	-	-	-	sends data
Traction Inverter	-	-	-	-	-	-	-	sends data
Motor	-	-	-	-	-	-	-	-
Cooling System	-	-	-	-	-	-	-	sends data
Brakes Controller	-	-	-	-	-	-	-	sends data
Telemetry Unit	-	-	updates limits	sends commands	-	sends target rates	sends commands	-

Table 2.7: Data connection matrix

2.4.6 Final system description

Our inverter:

A precharge circuit:

The MSD: We buy the devices from Amphenol

2.4.7 Manufacturing process

Our PCB Design

PCBs

Prototyping: Prototype PCBs are fabricated in the FabLab associated with our university. The FabLab provides access to PCB manufacturing equipment and materials, enabling the rapid production of prototypes for initial testing and design validation. Once the PCBs are fabricated, they are assembled manually by our team members.

Production: We ordered our final PCBs from JLCPCB, a leading PCB manufacturing service. In addition to JLCPCB, we also collaborate with Würth Elektronik who produce PCBs in Germany, aligning with our goal of sustainability.

Inverter

The inverter is a product from Leadrive used as an OEM product in automotive and mobility industry.

Support from Leadrive: The development of the inverter system is supported by Leadrive, a company specializing in advanced inverter technology. Their expertise significantly contributes to the optimization of our propulsion system. Collaboration with Formula Student Team of FH Aachen: Additionally, we collaborate with the Formula Student Team of FH Aachen, benefiting from their practical experience in electric vehicle design and inverter application. This partnership enriches our project with valuable insights into inverter integration and performance enhancement.

2.4.8 Testing

We started testing software.

2.5 Sensing and Control

2.5.1 Overview

Our S&C subsystem consists of a

- Control Boards:
  - Braking Controller
  - Thermal (Cooling) Controller
- Telemetry Device:
  - CAN Bus
  - Telemetry Transceiver
  - Network Transceiver
  - GUI/Logging system

In this section, the main components of the sensor network and software architecture shall be described, as well as their basic functionality. A special focus shall be made on how safety mechanisms are implemented in these systems. Extensive design descriptions are expected for, if applicable:

2.5.2 Control Boards

Introduction

1. Brief overview of all control boards (Brakes, Thermal)
2. Diagram with the connection of all boards with NAP and control station.
3. Brief description of communication protocols used.

Parts Lists

Example Thermal Parts list start: Parts List:

Amount	Name	Company (Serial Number)	Dimensions (mm
38	Additional Temperature Sensors (NTC, 10k Ohm)	Mouser	1000 x
1	Coolant Pump	Unknown	Unkno
1	MOSFET Bridge	Unknown	Unkno

Table 2.8: Description of Components

2.5.3 State Machine of the Vehicle

Our states are different for each component.

2.5.4 Code Architecture and Class Diagram

Brakes Controller

The software follow a simple state:

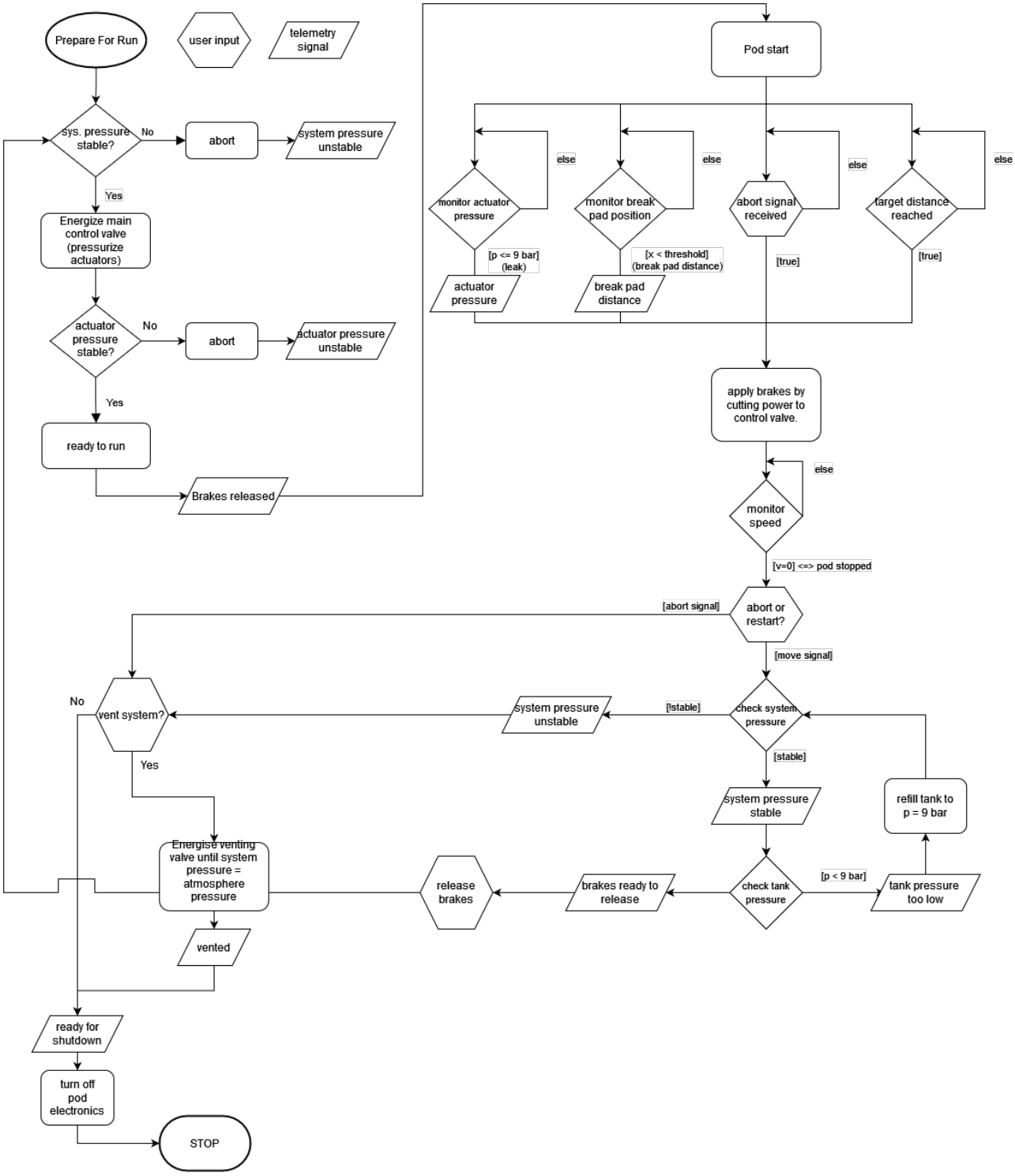

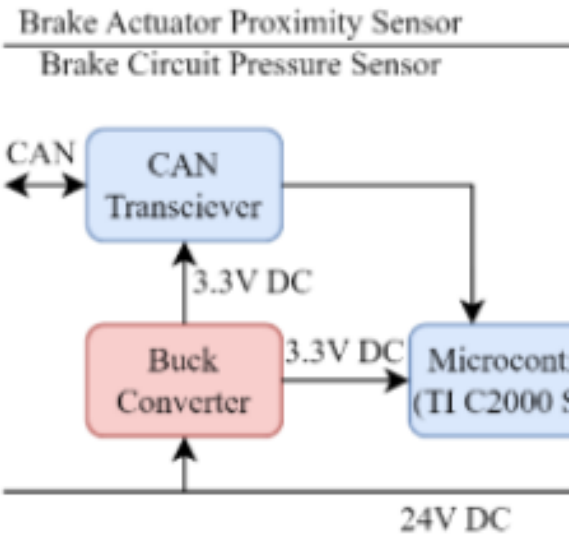

The implementation of the hardware architecture goes as follows:

Thermal Controller

it follows the following state diagram:
— INSERT STATE DIAGRAM —

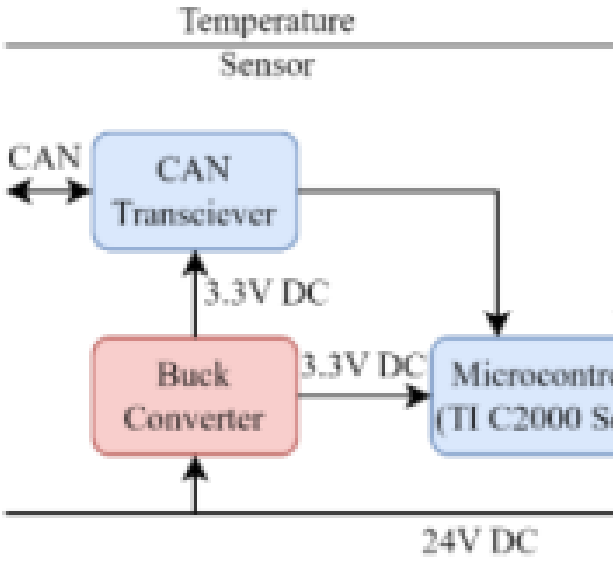

The following hardware architecture is to be implemented:

2.5.5 Control Boards/Units in the Vehicle

1. Brakes Controller Lacking. To be added.
2. Thermal Controller The Thermal Management Controller is responsible for cooling the Traction Components, i.e., Motor and Traction Controller. The actuator is the coolant pump which is controlled with the feedback of the temperature of coolant in the cooling loop. The Pump Speed is controlled via PWM to the MOSFET Bridge. The PWM duty cycle is simply calculated from a lookup table that is referenced to the temperature difference between target and actual temperatures. The only safety feature to be developed is to issue an emergency stop signal to HV Systems in the event the coolant temperature exceeds a critical temperature.

Parts List

Part	Manufacturer	Description
Raspberry Pi Zero 2 W	Raspberry	Microcontroller for telemetry
Raspberry Pi 4 B	Raspberry	Computer for telemetry
MC3479	Memsic	3-Axis Accelerometer
RS485 CAN HAT	Waveshare	CAN adapter for RPI4B

Table 2.9: Telemetry System Parts List

2.5.6 Integration with other systems

The friction brakes, the cooling pump and the motor are controlled through our system.

2.5.7 Graphical User Interface (GUI)

2.5.8 Telemetry Device

For communication and navigation, we use our telemetry system, that consists of a CAN bus, a CAN2WLAN transmitter and a VCU.

Introduction

1. Brief overview of Telemetry Components
2. Diagram with the connection of all boards with NAP and control station.
3. Explanation of the Signals Transmitted

Parts Lists

2.6 Additional considerations when writing the document for specific subsystems

Sources:

- https://link.springer.com/article/10.1007/s40789-022-00494-0 BMS System Reliability
-